

mqix.pis: A toolbox for quantum dynamics simulation of spin ensembles in Dicke basis

Nguyen Tan Viet,¹ Nguyen Thi Chuong,² Vu Thi Ngoc Huyen,³ and Le Bin Ho^{4,5}

¹*FPT University, Hanoi, Vietnam**

²*ILotusLand VietNam, Hochiminh City, Vietnam*

³*Center for Computational Materials Science, Institute for Materials Research, Tohoku University, Sendai, Miyagi 980-8577, Japan*

⁴*Frontier Research Institute for Interdisciplinary Sciences, Tohoku University, Sendai 980-8578, Japan*

⁵*Department of Applied Physics, Graduate School of Engineering, Tohoku University, Sendai 980-8579, Japan[†]*

(Dated: January 31, 2023)

We introduce `mqix.pis`, a library of `mqix`, for quantum dynamics simulation of spin ensembles. The library emulates a dynamic process by a quantum circuit, including initializing a quantum state, executing quantum operators, and measuring the final state. It utilizes collective processes in spin ensembles to reduce the dimension from exponentially to quadratically with the number of particles, i.e., the quantum state spans in Dicke basis. It also facilitates the simulation time with multi-core processors and Graphics Processing Units. The library is thus applicable for the simulation of ensembles of large number of particles that have collective properties. Various phenomena, such as spin squeezing, variational quantum squeezing, quantum phase transition, and many-body quantum dynamics, can be simulated using the library.

Note for installation: Download the source code and run: `pip3 install .`
Or install from PyPI, run: `pip3 install mqix`
Official website: <https://vqisinfo.wixsite.com/mqix>
<https://mqix-developers.readthedocs.io/en/latest/index.html>
<https://pypi.org/project/mqix/>

I. INTRODUCTION

The toolbox `mqix` is a Python-based simulation package for quantum measurement and applications in quantum metrology and quantum tomography [1]. The package allows for designing quantum systems (state and operators) and performing quantum measurements. It embeds various conventional measurement operators, including Pauli, Stoke, MUB-POVM, and SIC-POVM, with two backends to simulate the measurement results. The applications in quantum metrology and quantum tomography were reported so far.

In this version, we introduce a new library called `mqix.pis` for programmable quantum dynamics of spin ensembles with collective processes. In the collective processes, an N -particle state spans in Dicke basis with $O(N^2)$ -dimension, smaller than the product 2^N -dimension [2]. This is the backbone for the simulation of a large number of particles with low computation costs. Thus, the library is restricted to the simulation of collective phenomena in ensemble systems with collective processes [3], which is different from a general simulation method, where every particle (qubit) is accessible.

The library executes a dynamic simulation by a quantum circuit with a sequence of initialization collective state, the action of collective operators, and measurements in the Dicke basis. It supports parallelizing multi-

core processors and Graphics Processing Units (GPUs) to facilitate the running time. In terms of application, it is suitable for studying spin squeezing [4], variational quantum squeezing [5, 6], quantum phase transition [7], many-body quantum dynamics [8], and other quantum algorithms that have collective properties. The library is adaptable to simulate collective phenomena in various physical platforms, such as trapped ions [9], ultracold atoms in optical lattices [10], Rydberg atom arrays in optical tweezers [5], and nitrogen-vacancy centers [11].

This paper is organized as follows. Section II introduces quantum computing with collective processes in ensembles of two-level systems. Section III details the structure of `mqix.pis` library and its benchmark results are given in Section IV. Section V is devoted to applications on spin squeezing and quantum phase transition. A brief conclusion is given in Section VI. The full code for generating figures in the paper can be found in the Appendices.

II. QUANTUM COMPUTING WITH COLLECTIVE PROCESSES IN ENSEMBLES OF TWO-LEVEL SYSTEMS

A. Collective processes in ensembles of two-level systems

Consider an ensemble of N two-level particles characterized by the single and collective angular momentum operators $J_\alpha^{(n)} = \frac{1}{2}\sigma_\alpha^{(n)}$ and $J_\alpha = \sum_n J_\alpha^{(n)}$, respectively, where σ_α , $\alpha = \{x, y, z\}$, are Pauli matrices.

* Electronic address: vietnthe153763@fpt.edu.vn

[†] Electronic address: binho@fris.tohoku.ac.jp

The joint Hilbert space of the ensemble is a composite $\mathcal{H}_E = \mathcal{H}^{(1)} \otimes \dots \otimes \mathcal{H}^{(N)}$ with $\dim(\mathcal{H}_E) = 2^N$. A generic mixed state is given by a $(2^N \times 2^N)$ -matrix as

$$\rho = \sum_{\substack{m_1, m_2, \dots, m_N \\ m'_1, m'_2, \dots, m'_N}} \rho_{m_1, m_2, \dots, m_N; m'_1, m'_2, \dots, m'_N} \times |m_1, m_2, \dots, m_N\rangle \langle m'_1, m'_2, \dots, m'_N|, \quad (1)$$

where the product basis is $|m_1, m_2, \dots, m_N\rangle = |m_1\rangle \otimes |m_2\rangle \otimes \dots \otimes |m_N\rangle$, with $m_n = \pm \frac{1}{2}$ are eigenvalues of $J_z^{(n)}$.

Under the collective processes [3, 12], the product basis is represented by an irreducible representation (irrep) basis $\{|j, m, i\rangle\}$, where $j \leq N/2$ is the total angular momentum with $j_{\min} = \text{mod}(N/2)/2$, $j_{\max} = N/2$, and $|m| \leq j$. The quantum number $i = 1, \dots, d_N^j$ distinguishes d_N^j degenerate irreps, where

$$d_N^j = \frac{N!(2j+1)}{(N/2-j)!(N/2+j+1)!} \quad (2)$$

is the number of ways to combine N particles that gets the total angular momentum j [13]. The quantum state is recast in the irrep basis as

$$\rho = \sum_{\substack{j, m, i \\ j', m', i'}} \rho_{jmi, j'm'i'} |j, m, i\rangle \langle j', m', i'|. \quad (3)$$

The state ρ is permutation invariant (PI) if it does not change under a permutation operator P_π of a permutation π , i.e., $P_\pi \rho P_\pi^\dagger = \rho \forall \pi$ [14]. Decompose P_π into the multiplicity subspaces $\mathcal{H}_j \otimes \mathcal{K}_j$ following the Schur-Weyl duality [15] as $P_\pi = \bigoplus_{j=j_{\min}}^{j_{\max}} \mathbf{I}_{\mathcal{H}_j} \otimes P_j(\pi)$, where $\bigoplus_{j=j_{\min}}^{j_{\max}} \mathcal{H}_j \otimes \mathcal{K}_j = \mathcal{H}_E$, $\dim(\mathcal{H}_j) = 2j+1$ and $\dim(\mathcal{K}_j) = d_N^j$, that P_π only acts on the irrep subspace \mathcal{K}_j , which causes a general permutation symmetry, i.e., $\rho_{jmi, j'm'i} = \rho_{jmi, j'm'i'} \forall i, i' \in [1, d_N^j]$, then a permutation-invariant state is given by

$$\rho_{\text{PI}} = \bigoplus_{j=j_{\min}}^{j_{\max}} \rho_j \otimes \mathbf{I}_{\mathcal{K}_j} = \sum_{j, m, m'} \rho_{jmm'} |j, m\rangle \langle j, m'| \otimes \mathbf{I}_{\mathcal{K}_j}. \quad (4)$$

Hence, we can ignore the identical irrep label i and recast the state in a collective form as [3]

$$\rho_C = \bigoplus_{j=j_{\min}}^{j_{\max}} \rho_j = \sum_{j, m, m'} \rho_{jmm'} |j, m\rangle \langle j, m'|, \quad (5)$$

where the effective amplitude $\rho_{jmm'}$ and the effective density matrix elements $|j, m\rangle \langle j, m'|$ are given by

$$\rho_{jmm'} |j, m\rangle \langle j, m'| = \frac{1}{d_N^j} \sum_{i=1}^{d_N^j} |j, m, i\rangle \langle j, m', i|. \quad (6)$$

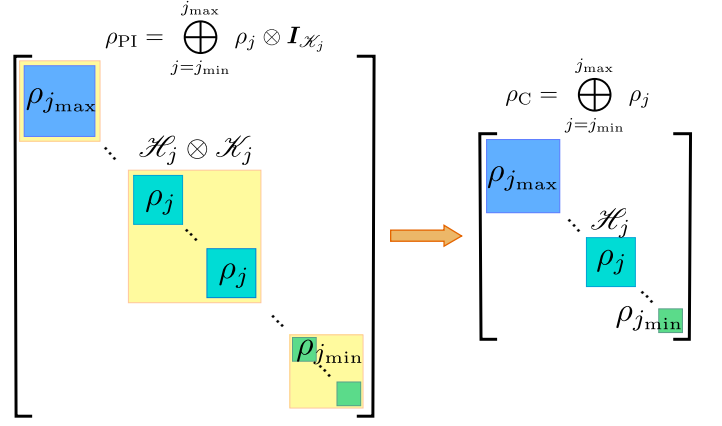


Figure 1. Block-diagonal structure of a quantum state in the irrep representation with permutation invariant (left) and its corresponding in the collective representation (right). Each yellow block represents the subspace $\mathcal{H}_j \otimes \mathcal{K}_j$ and contains d_N^j identical density matrices ρ_j . In the collective form, we ignore the identity of density matrices by removing the subspace \mathcal{K}_j .

The effective basis $\{|j, m\rangle\}$ is known as the Dicke basis [2], i.e., $|j, m\rangle = \frac{1}{\sqrt{d_N^j}} \sum_{i=1}^{d_N^j} |j, m, i\rangle$, that is the eigenstates of the collective angular momentum operators

$$\mathbf{J}^2 |j, m\rangle = j(j+1) |j, m\rangle, \quad (7)$$

$$J_z |j, m\rangle = m |j, m\rangle, \quad (8)$$

$$J_\pm |j, m\rangle = \sqrt{(j \mp m)(j \pm m + 1)} |j, m \pm 1\rangle, \quad (9)$$

where $\mathbf{J}^2 = J_x^2 + J_y^2 + J_z^2$ and $J_\pm = J_x \pm iJ_y$. The collective angular momentum operators obey the commuting relation

$$[J_\alpha, J_\beta] = i\epsilon_{\alpha\beta\gamma} J_\gamma, \quad (10)$$

where $\{\alpha, \beta, \gamma\} \in \{x, y, z\}$, and $\epsilon_{\alpha\beta\gamma}$ is the Levi-Civita symbol.

Under the collective processes, the Hilbert space \mathcal{H}_N reduces to a collective subspace $\mathcal{H}_C \sim O(N^2) \subset \mathcal{H}_E$ as [3, 12]

$$\begin{aligned} \dim(\mathcal{H}_C) &= \bigoplus_j \dim(\mathcal{H}_j) \\ &= \begin{cases} (N+3)(N+1)/4, & \text{for odd } N, \\ (N+2)^2/4, & \text{for even } N. \end{cases} \end{aligned} \quad (11)$$

Notable that both the PI and collective states have the j -irrep block-diagonal structure where all degeneracy with the same j are presented in the same block. See figure 1 for the block-diagonal structure of these quantum states. Similarly, the collective angular momentum operators $\{J_\alpha\}$ are represented by block-diagonal of spin- j operators $\{S_\alpha^{(j)}, \forall j \in [j_{\min}, j_{\max}]\}$.

Especially in the symmetry group [16–18], a symmetry mixed state is a particular case of the collective state with

$\rho_{jmm'} = 0$ for $j \neq N/2$ and is presented in the first j -irrep block $\mathcal{H}_{N/2}$ with the dimension $\dim(\mathcal{H}_{N/2}) = N + 1$. The symmetry states characterize the ensemble phenomena of multiparticle, such as entanglement [14, 16], spin-squeezing [19, 20], and zero-temperature quantum phase transitions [21–25].

B. Collective quantum states

An important collective quantum state is the ground state where all spins are down, i.e., $|g\rangle^{\otimes N} = |\downarrow \cdots \downarrow\rangle$. In the Dicke basis, it gives $|g\rangle^{\otimes N} = |\frac{N}{2}, -\frac{N}{2}\rangle$ and its density matrix locates in the bottom-right position of

the first irrep block. Another one is the excited state, $|e\rangle^{\otimes N} = |\uparrow \cdots \uparrow\rangle$, which is given by $|e\rangle^{\otimes N} = |\frac{N}{2}, \frac{N}{2}\rangle$, and the density matrix locates on the top-left of the first irrep block. An entangled GHZ state is a superposition of the ground and excited states as

$$|\text{GHZ}\rangle = \frac{1}{\sqrt{2}} \left(\left| \frac{N}{2}, \frac{N}{2} \right\rangle + \left| \frac{N}{2}, -\frac{N}{2} \right\rangle \right). \quad (12)$$

Besides, a literature well-known coherent spin state (CSS) is a product state that resembles a coherent state of a classical harmonic oscillator [26, 27]. It explicitly expands in terms of a linear combination of $|\frac{N}{2}, m\rangle$ elements as

$$|\theta, \phi\rangle_{\text{CSS}} = \sum_{m=-\frac{N}{2}}^{\frac{N}{2}} \sqrt{\binom{N}{\frac{N}{2}+m}} \left(\cos \frac{\theta}{2} \right)^{\frac{N}{2}+m} \left(\sin \frac{\theta}{2} e^{-i\phi} \right)^{\frac{N}{2}-m} \left| \frac{N}{2}, m \right\rangle, \quad (13)$$

where $0 \leq \theta \leq \pi$ is the polar angle, and $0 \leq \phi \leq 2\pi$ denotes the azimuth angle in the spherical coordinates.

We emphasize that all these states obey the symmetry and are thus represented in the subspace $\mathcal{H}_{N/2}$. However, under noise, such as decoherence, symmetry states decay from the maximum j_{max} -irrep block and transfer to the lower blocks, resulting in the full collective subspace \mathcal{H}_C . (See Ref. [12] for an example.)

C. Collective operators

Collective operators are unitary transformations over all particles of the ensemble. We first introduce the rotation operator denoted by $R_{\mathbf{n}}(\theta, \phi)$. It rotates the original state counterclockwise by a polar angle θ around the xy plane and then by an angle ϕ around the z axis [4]

$$R_{\mathbf{n}}(\theta, \phi) = e^{-i\theta \mathbf{J} \cdot \mathbf{n}} = \exp[i\theta(J_x \sin \phi - J_y \cos \phi)], \quad (14)$$

where $\mathbf{J} = (J_x, J_y, J_z)$, $\mathbf{n} = (-\sin \phi, \cos \phi, 0)$, and $\mathbf{J} \cdot \mathbf{n} = \mathbf{J} \cdot \mathbf{n}$. For example, a CSS state can be prepared from the rotation $R_{\mathbf{n}}(-\theta, \phi)$ of the ground state, i.e., $|\theta, \phi\rangle_{\text{CSS}} = R_{\mathbf{n}}(-\theta, \phi) |\frac{N}{2}, -\frac{N}{2}\rangle$ [27]; or an excited state is given by a rotation $R_{\mathbf{n}}(\pi, \phi) |\frac{N}{2}, -\frac{N}{2}\rangle$. Specific cases of the rotation operator are rotation around the α axis, $\alpha \in \{x, y, z\}$ as

$$R_{\alpha}(\theta) = e^{-i\theta J_{\alpha}}. \quad (15)$$

These rotations allow us to transform quantum states everywhere in the spherical representation but not deform the states.

Hereafter, let us introduce other classes of transformation based on the nonlinear interactions that can deform the quantum states. They include one-axis twisting (OAT) [19, 28–34], two-axis countertwisting (TAT)

[19, 35–38], twist-and-turn (TNT) [39–42], and an important global Mølmer-Sørensen operator (GMS) [43–47].

An OAT transformation along the α axis is defined by

$$U_{\text{OAT}} = e^{-it\chi J_{\alpha}^2}, \quad (16)$$

where through the paper, we use $\hbar = 1$, χ is the nonlinearity interparticle interaction, and t is the time. It leads to a rotation proportional to J_{α} , $\alpha \in \{x, y, z\}$ and twist the quantum fluctuations of the ensemble. Similarly, a TAT transformation is defined by

$$U_{\text{TAT}} = e^{-it\chi(J_{\alpha}^2 - J_{\beta}^2)}, \quad (17)$$

where $\{\alpha, \beta\} \in \{x, y, z, +, -\}$. Next, for the TNT transformation, we have

$$U_{\text{TNT}} = e^{-it(\chi J_{\alpha}^2 - \Omega J_{\beta})}, \quad (18)$$

where Ω is the linearly coupling strength. Set $\Lambda = N\chi/\Omega$, then for $\chi \ll \Omega$, the TNT transformation reduces to the OAT one. Finally, the definition of a global Mølmer-Sørensen transformation is an entangling gate that operates on all particles of the ensemble [48]

$$U_{\text{GMS}} = e^{-i\theta(J_x \cos \phi + J_y \sin \phi)^2}. \quad (19)$$

It encompasses the pairwise and is given by two angles θ and ϕ . For $\theta = \pi/2$, the GMS gate is maximally entangling, i.e., GHZ state [43].

These transformations deform the collective states and result in the entangled or squeezed effect in the ensemble systems and thus exhibit various applications from quantum-enhanced meteorology [49–52] to quantum sensors, and atomic clocks [6, 53]. Besides, other transformations for creating highly quantum-enhanced states

include light-to-atoms transformation [54–59], quantum nondemolition measurement (QND) [49, 60–65], and adiabatically quantum phase transition [66–68], to name a few.

D. Depolarizing noise in the collective systems

Depolarizing noise is a typical type of quantum noise [69]. It can be defined through bit-flip, phase-flip, and bit-phase-flip channels for every single particle in the circuit [70]. Let $\rho = \sum_{j,m,m'} \rho_{jmm'} |j, m\rangle \langle j, m'|$ is the initial quantum state. Through a depolarizing channel applied to all particles in the ensemble, the state transforms to [69]

$$\rho_1 = (1 - \epsilon)\rho + \sum_{n=1}^N \left(\epsilon_x J_x^{(n)} \rho J_x^{(n)} + \epsilon_y J_y^{(n)} \rho J_y^{(n)} + \epsilon_z J_z^{(n)} \rho J_z^{(n)} \right), \quad (20)$$

where $0 \leq \epsilon \leq 1$ is the depolarized probability, and ϵ_i , $i \in \{x, z, y\}$ are the probabilities the of bit-flip, phase-flip, and bit-phase-flip errors, respectively. In this paper, we restrict to symmetry noise channels, i.e., $\epsilon_x = \epsilon_y = \epsilon_z = \epsilon'$. Here, ϵ' obeys the normalized condition that $\text{tr}(\rho_1) = 1$, or $\epsilon' = \epsilon / \text{tr} \left[\sum_{n=1}^N (J_x^{(n)} \rho J_x^{(n)} + J_y^{(n)} \rho J_y^{(n)} + J_z^{(n)} \rho J_z^{(n)}) \right]$. Substituting

$$J_x^{(n)} = \frac{1}{2} (J_+^{(n)} + J_-^{(n)}); \quad J_y^{(n)} = \frac{-i}{2} (J_+^{(n)} - J_-^{(n)}) \quad (21)$$

into Eq. (20) and set

$$\rho' = \sum_{n=1}^N \left[\frac{1}{2} (J_+^{(n)} \rho J_-^{(n)} + J_-^{(n)} \rho J_+^{(n)}) + J_z^{(n)} \rho J_z^{(n)} \right], \quad (22)$$

we rewrite Eq. (20) as

$$\rho_1 = (1 - \epsilon)\rho + \epsilon \frac{\rho'}{\text{tr}(\rho')}. \quad (23)$$

Following Refs. [3, 12, 71, 72], we derive the terms $\sum_{n=1}^N J_k^{(n)} |j, m\rangle \langle j, m'| J_l^{(n)\dagger}$ for all $\{k, l\} \in \{+, -, z\}$, and compute ρ_1 straightforwardly.

Under the noise, the permutation symmetry in the system is broken, resulting in a deviation from $|j, m\rangle$ to $|j \pm 1, m \pm 1\rangle$. Thus, the final state spans in the collective Hilbert space \mathcal{H}_C with all j -irrep blocks for all $j_{\min} \leq j \leq j_{\max}$.

In Sec. III, we introduce `tcix.pis` library for quantum dynamics simulation of ensemble systems in the Dicke basis based on the theoretical framework described here.

III. QUANTUM SIMULATION WITH COLLECTIVE PROCESSES IN ENSEMBLES OF TWO-LEVEL SYSTEMS

The simulation is based on `tcix` package, a quantum toolbox for quantum measurement, metrology, and tomography [1]. Here, we develop `tcix.pis` library for simulating various quantum dynamics of spin ensembles in Dicke basis.

A. Features of the library

- Assist a large number of particles with the collective processes of the ensemble.
- Assist fast simulation with parallelizing multi-core processors and Graphics Processing Units (GPUs).

B. Structure of the program

A basic quantum circuit includes a quantum register (quantum state), quantum gates, and measurements. In `tcix.pis`, the computational basis is Dicke basis $|j, m\rangle \langle j, m|$, represented by a sparse matrix. The quantum register is a density matrix in the Dicke basis, initially prepared in the ground state, i.e., $\rho_0 = |\frac{N}{2}, -\frac{N}{2}\rangle \langle \frac{N}{2}, -\frac{N}{2}|$. This is a symmetry collective state spans in the subspace $\mathcal{H}_{N/2}$, and thus it has the dimension of $(N + 1) \times (N + 1) \ll 2^N \times 2^N$. This is a highlighted feature of the library that allows us to compute a large number of particles. Similarly, quantum gates are collective operators, e.g., K , that apply to the quantum register and transform it into the evolved state

$$\rho = K \rho_0 K^\dagger. \quad (24)$$

A list of build-in quantum gates and their syntax are given in Tab. I. These gates are represented by sparse matrices with the same dimension as the quantum register. Finally, the measurement on the Dicke basis gives the probability

$$P(j, m) = \text{tr}[\rho \cdot |j, m\rangle \langle j, m|] = \langle j, m | \rho | j, m \rangle. \quad (25)$$

To mimic the experiential probability, we apply the `cdf` back-end in `tcix` [1].

The following example code shows how to execute a simple quantum circuit with a rotation gate R_n using the circuit, `RN`, and `measure` functions in the library `tcix.pis`:

```
from tcix import *
from tcix.pis import *
import numpy as np

N = 50 #particles
qc = circuit(N) #create circuit
qc.RN(-np.pi/2, np.pi/4) #apply RN
```

Table I. List of basic quantum gates (function type) built in Gate class of the library `tcix.pis`. In each gate, the additional argument `*args` (float) allows to add the depolarized probability (noise parameter).

Name	Syntax	Description
R_x gate	<code>RX(θ, *args)</code>	Rotate the quantum state at an angle θ around the x axis, i.e., $RX(\theta) = e^{-i\theta J_x}$
R_y gate	<code>RY(θ, *args)</code>	Rotate the quantum state at an angle θ around the y axis, i.e., $RY(\theta) = e^{-i\theta J_y}$
R_z gate	<code>RZ(θ, *args,)</code>	Rotate the quantum state at an angle θ around the z axis, i.e., $RZ(\theta) = e^{-i\theta J_z}$
R_n gate	<code>RN(θ, ϕ, *args)</code>	$RN(\theta, \phi) = e^{-i\theta(J_x \sin \phi - J_y \cos \phi)}$
R_+ gate	<code>R_plus(θ, *args)</code>	$R_plus(\theta) = e^{-i\theta J_+}$
R_- gate	<code>R_minus(θ, *args)</code>	$R_minus(\theta) = e^{-i\theta J_-}$
R_x^2 gate	<code>RX2(θ, *args)</code>	$RX2(\theta) = e^{-i\theta J_x^2}$
R_y^2 gate	<code>RY2(θ, *args)</code>	$RY2(\theta) = e^{-i\theta J_y^2}$
R_z^2 gate	<code>RZ2(θ, *args)</code>	$RZ2(\theta) = e^{-i\theta J_z^2}$
OAT gate	<code>OAT(θ, gate_type, *args)</code> ----- $\theta = t\chi$: rotation angle gate_type = {'x', 'y', 'z'}	One-axis twisting gate, e.g., $OAT(\theta, 'x') = e^{-i\theta J_x^2}$
TAT gate	<code>TAT(θ, gate_type, *args)</code> ----- gate_type = ' $\alpha\beta$ ', $\forall \{\alpha, \beta\} \in \{x, y, z, plus, minus\}$	Two-axis twisting gate, e.g., $TAT(\theta, '\alpha\beta') = e^{-i\theta(J_\alpha^2 - J_\beta^2)}$
TNT gate	<code>TNT(θ, Λ, gate_type, *args)</code> ----- gate_type = ' $\alpha\beta$ ', $\forall \{\alpha, \beta\} \in \{x, y, z, plus, minus\}$	Twist and Turn gate, e.g., $TNT(\theta, \Lambda, '\alpha\beta') = e^{-i\theta(J_\alpha^2 - \frac{\Lambda}{\Lambda} J_\beta)}$
GMS gates	<code>GMS(θ, ϕ, *args)</code>	Global Mølmer-Sørensen gate, e.g., $GMS(\theta, \phi) = e^{-i\theta(J_x \cos \phi + J_y \sin \phi)^2}$

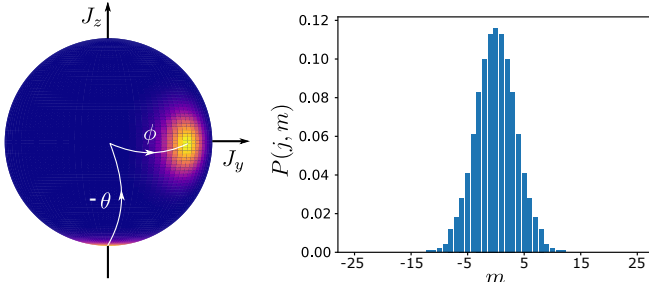


Figure 2. (Left) Husimi visualization for the circuit initially prepared in the ground state (the South pole) and then transferred into a CSS state by applying a rotation gate $RN(-\pi/2, \pi/4)$. (Right) Probability distribution $P(j, m)$ of the final state measuring on the Dicke basis $|j, m\rangle$. Plot for #particles $N = 50$.

```
prob = qc.measure(num_shots=1000) #measure
#to get state information
psi = qc.state #sparse matrix
psi = qc.state.toarray() #full matrix
```

The results are given in figure 2. The left figure is the Husimi visualization for the circuit's state initially

prepared in the ground state (the South pole). Under the rotation gate $RN(-\pi/2, \pi/4)$, the state rotates around the y axis at an angle $\theta = -\pi/2$ and then rotates around the z axis at an angle $\phi = \pi/4$. The final state becomes a CSS state, where its probabilities measured in the Dicke basis are exhibited in the right figure. (See the full code in A.)

To compute the expectation value of a given observable, such as J_z , we execute the `expval` function as

```
expJz = qc.expval('Jz')
```

We emphasize that the observable must obey the collective process, such as the collective angular momentum operators $\{J_\alpha\}$, for $\alpha \in \{x, y, z, +, -\}$. The program supports these observables $\{J_\alpha\}$ include 'Jx', 'Jy', 'Jz', 'J_plus', 'J_minus' and $\{J_\alpha^2\}$ include 'Jx2', 'Jy2', 'Jz2', 'J_plus2', 'J_minus2'. For an arbitrary self-defined observable, such as a linear combination of these listed observables, the users can compute manually from the quantum state and the self-defined observable. For example, the following script computes the expectation value of $J_x + J_y + J_z$

```
Jx = qc.Jx()
Jy = qc.Jy()
```

```
Jz = qc.Jz()
Js = Jx + Jy + Jz
psi = qc.state
expectJ = np.trace(psi@Js)
```

Finally, when we apply a quantum gate onto the circuit, it also causes noises due to the assumption of the imperfection of the gate. In the current version of the library, we restrict to the typical depolarizing noise as described in subsection IID. To include the noise, we use noise option in the quantum gate function, which is the depolarized probability (or noise parameter) ϵ . For example, we add the noise with $\epsilon = 0.01$ into the RN gate as following

```
qc.RN(-np.pi/2,np.pi/4, noise = 0.01)
```

C. Additional options for running multi-core processors and GPUs

By default, the program executes on CPUs with one processor. However, it also allows for running parallel multi-core processors, which assists the running time. Technically, we use the python multiprocessing module to create multiple processors for handling different parts of the input list. To execute the program in multi-core processors, we add the option `num_process` into the circuit. This is an integer number stands for the number of processors. For example, one can create a quantum register with 50 particles and run it with 25 processors by using the following command

```
qc = circuit(N = 50, num_process = 25)
```

Similarly, the library supports running on GPU devices, which can outperform the CPUs in some cases. To execute the program with GPUs, we add the option `use_gpu` into the circuit. For example,

```
qc = circuit(N = 50, use_gpu = True)
```

Note that to run with GPUs, the users must turn off the option `num_process` or leave it as one. In GPUs, the sparse-matrix structure will convert into the tensor structure using `pyTorch` library.

IV. BENCHMARK RESULTS

For benchmarking the library, we consider the execution time versus the number of particles N . The benchmarking circuit is shown in Fig. 3(a), which consists of a set of rotation gates $\{R_x, R_y, \text{ and } R_z\}$ with L times and the measurement of the final state. The running time versus N for $L = 3$ is shown in Fig. 3(b). For the noiseless case (filled diamond), the circuit executes up to $N = 200$, consuming around 3 seconds with 1 processor CPU (see the inset Fig. 3(b)). The complexity is $\mathcal{O}(N^3)$. Under the presence of noise, the running time rapidly increases with N . The complexity is $\mathcal{O}(N^7)$ for

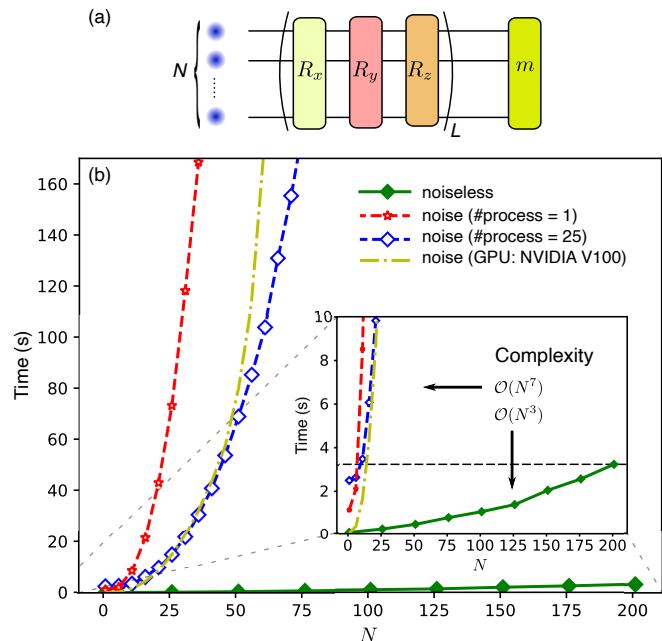


Figure 3. (a) Benchmarking quantum circuit. The circuit consists of N particles, transfers under L layers of rotation gates R_x, R_y, R_z , and measures in the Dicke basis. (b) The running time versus the number of particles N for different cases of with/without noise and CPUs/GPUs. Inset: zoom in the y axis from 0 to 10 seconds. The results are shown for $L = 3$.

CPU regardless of the number of processors. Nevertheless, by using multi-processing on CPUs, we can reduce the running time of adding noise by p times, with p being the computer's maximum processors. Hence, the running time for 25 processors (open diamond) is faster than the 1 processor (open star).

We next evaluate the performance of the GPU (NVIDIA V100) (dashed-dot curve) and compare it with the 25-processor CPU. The complexity performing on the GPU is $\mathcal{O}(N^7)$. For $N < 25$, it offers a better running time, while increasing N will slow down the running time. This result relies on the different matrix structures in these two devices, i.e., the CPU uses sparse matrices, whereas the GPU uses tensor matrices. For small N , the tensor dimension is small, the GPU thus displays its advantage overcome the CPU, and for larger N , the tensor dimension increases while the sparse matrices are unaffected. As a result, the performance of CPU gradually overcomes the GPU. The full code for producing Fig. 3 is given in B.

The time complexities of a quantum circuit with various cases are listed in Tab. II. We evaluate the complexity by analyzing the number of operations performed on the code's statements. Details are given in C.

Finally, we compare `qix.pis` library with other libraries including `qsim` [73], `cirq` [74], `qulacs` [75], `yao` [76], `qsun` [77], `quest` [78], `pennylane` [79], `qiskit` [80], `projectQ` [81], and `qypuil` [82]. The results are shown in Fig. 4. We

Table II. The complexities of a quantum circuit for different cases as shown in the list.

	Noiseless	Noisy
Symmetry state	$\mathcal{O}(N^3)$	$\mathcal{O}(N^6)$
Collective state	$\mathcal{O}(N^6)$	$\mathcal{O}(N^7)$

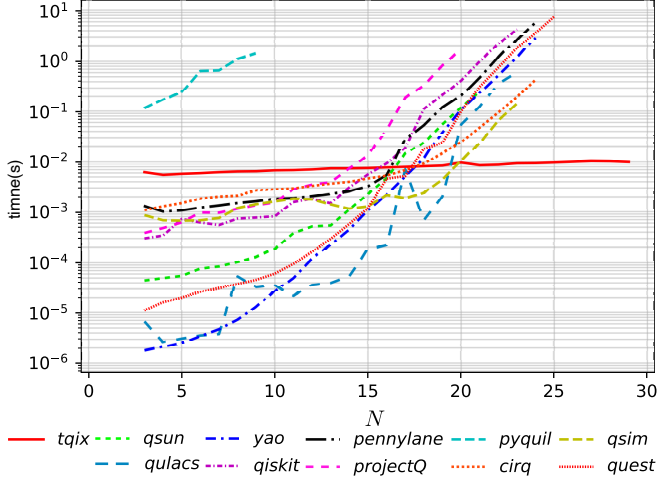


Figure 4. Comparison of the running time between various libraries. The benchmarking circuit is the one that generates a GHZ state.

consider a quantum circuit that generates the maximum entanglement GHZ state. In `tqix.pis`, a GHZ state is created by applying the $\text{GMS}(\pi/2, 0)$ gate onto the initial ground state. In other libraries, the circuit encompasses one Hadamard gate and $N - 1$ CNOT gates. For $N < 30$ as shown in the figure, `tqix.pis` remains the running time lower than 10^{-2} seconds while the time for others increases exponentially versus N . See the full code in D. The `tqix.pis` represents quantum states and operators by sparse matrices; thus, it consumes a certain running time and less depend on (small) N . The other libraries represent quantum states by state vectors, where the running time depends on 2^N .

Note that in this comparison, we aim to emphasize different perspectives for different simulation libraries: while previous libraries use full Hilbert space to perform general quantum simulation framework, our library applies the collective Hilbert subspace to simulate collective phenomena in ensemble systems.

V. APPLICATIONS

A. Spin squeezing

Definition. There are several definitions for the squeezing parameter in the literature [4, 19, 29, 83]. The two well-known spin squeezing parameters are given by Kitagawa and Ueda [19] and Wineland [83]. According to Kitagawa and Ueda, the spin-squeezing state (SSS)

redistributes quantum fluctuations between two noncommuting observables while preserving the minimum uncertainty product [3, 12]. The corresponding squeezing parameter is given by

$$\xi_S^2 = \frac{2}{N} \left[\langle \mathbf{J}_{n_2}^2 + \mathbf{J}_{n_3}^2 \rangle \pm \sqrt{\langle \mathbf{J}_{n_2}^2 - \mathbf{J}_{n_3}^2 \rangle^2 + 4\text{cov}^2(\mathbf{J}_{n_2}, \mathbf{J}_{n_3})} \right], \quad (26)$$

where

$$\begin{aligned} \mathbf{n}_2 &= (-\sin \phi, \cos \phi, 0); \\ \mathbf{n}_3 &= (\cos \theta \cos \phi, \cos \theta \sin \phi, -\sin \theta), \end{aligned}$$

and

$$\begin{aligned} \theta &= \arccos \left(\frac{\langle J_z \rangle}{|\mathbf{J}|} \right), \\ \phi &= \begin{cases} \arccos \left(\frac{\langle J_x \rangle}{|\mathbf{J} \sin \theta|} \right) & \text{if } \langle J_y \rangle > 0, \\ 2\pi - \arccos \left(\frac{\langle J_x \rangle}{|\mathbf{J} \sin \theta|} \right) & \text{if } \langle J_y \rangle \leq 0, \end{cases} \end{aligned} \quad (27)$$

with $|\mathbf{J}| = \sqrt{\langle J_x \rangle^2 + \langle J_y \rangle^2 + \langle J_z \rangle^2}$. These notations are given in the spherical coordinate. The covariant $\text{cov}(\mathbf{J}_{n_2}, \mathbf{J}_{n_3})$ is given by

$$\text{cov}(\mathbf{J}_{n_2}, \mathbf{J}_{n_3}) = \frac{1}{2} \langle [\mathbf{J}_{n_2}, \mathbf{J}_{n_3}]_+ \rangle - \langle \mathbf{J}_{n_1} \rangle \langle \mathbf{J}_{n_2} \rangle. \quad (28)$$

Similarly, the Wineland squeezing parameter is defined by [83]

$$\xi_R^2 = \left(\frac{N}{2|\langle \mathbf{J} \rangle|} \right)^2 \xi_S^2. \quad (29)$$

When $\xi^2 < 1$, the system state is squeezed.

In `tqix.pis`, to compute the squeezing parameters, we call `get_xi_2_S` and `get_xi_2_R` functions for ξ_S^2 and ξ_R^2 , respectively. For example, we generate a quantum circuit with $N = 50$ particles and calculate its squeezing parameters as follows:

```
qc = circuit(N = 50)
xiS2 = get_xi_2_S(qc)
xiR2 = get_xi_2_R(qc)
```

Spin squeezing by nonlinear gates. Spin squeezing state (SSS) can be created from the CSS by applying a nonlinear gate such as OAT, TNT, and TAT. Here, we illustrate the spin squeezing for these three cases using `tqix.pis` as follows. First, we apply the rotation gate $\text{RN}(\pi/2, 0)$ onto the initial quantum register to transform the ground state into the CSS state. Then, we apply different nonlinear gates, including $\text{OAT}(\theta)$, $\text{TNT}(\theta)$ and $\text{TAT}(\theta, N/2)$. We calculate the squeezing parameters of the final states in these cases and show the result in figure 5. In the left figure, we plot $\xi_S^2(\text{dB})$ and $\xi_R^2(\text{dB})$. There exhibit squeezing for all cases, i.e., $\xi^2(\text{dB}) < 0$, and there exists a lower bound for each squeezing parameter at a certain θ . The ξ_R^2 's curves are always higher than ξ_S^2 since $\frac{N}{2} \geq |\langle \mathbf{J} \rangle|$ in Eq. (29). The corresponding Husimi

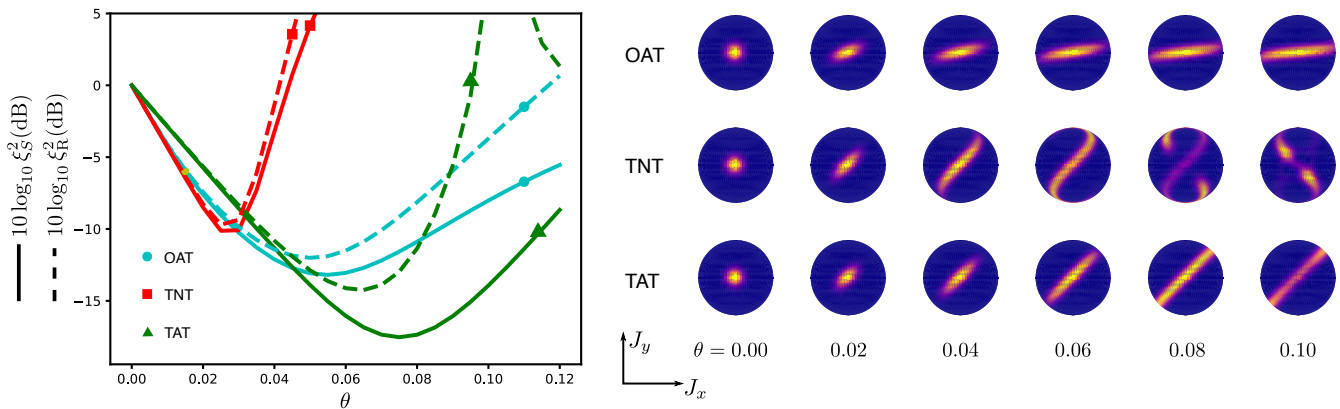


Figure 5. (left) Spin squeezing parameters ξ_S^2 and ξ_R^2 (in dB) are generated by OAT, TNT, and TAT gates. There exist an optimal θ so that the squeezing reaches the maximum. (right) The corresponding Husimi visualization for several values of θ . The figure is plotted at $N = 100$ particles.

visualizations are shown in the right figure for several values of θ , in which displace different types of squeezing due to different types of nonlinear gate (OAT, TNT, and TAT). We plot the results for $N = 100$ particles. See the full code in E.

Spin squeezing by variational algorithms. It can be seen from the previous results, these squeezing parameters reflect the presence of an optimal SSS when tuning to the right θ , so it is reasonable to use optimization algorithms to find optimal circuit's parameters corresponding to the minimum of squeezing function. Here, we introduce a quantum-classical hybrid variational scheme. In the quantum part, we sequentially apply a set of OAT(θ_1), TNT (θ_2), and TAT($\theta_3, N/2$), into a CSS circuit. We then measure the final state on the Dicke basis and send the results into the classical part to compute the cost function. For generating SSS, we apply the cost function to be the squeezing parameter

$$\mathcal{C}(\boldsymbol{\theta}) = \xi_S^2(\boldsymbol{\theta}), \quad (30)$$

where $\boldsymbol{\theta} = (\theta_1, \theta_2, \theta_3)$. We solve the following optimization problem

$$\boldsymbol{\theta}^* = \arg \min_{\boldsymbol{\theta}} \mathcal{C}(\boldsymbol{\theta}), \quad (31)$$

by using gradient-based optimizes including gradient descent (GD), Adam, and quantum natural gradient descent (QNG) (see F for the details.) The gradient of \mathcal{C} with respect to $\theta \forall \theta \in \boldsymbol{\theta}$ is derived by a finite difference (findiff) approximation for sparse matrix type (use in CPUs)

$$\frac{d\mathcal{C}}{d\theta_i} \approx \frac{\mathcal{C}(\theta_i + \epsilon) - \mathcal{C}(\theta_i - \epsilon)}{2\epsilon}, \quad (32)$$

which small ϵ , and by an automatic differential (autodiff) mechanism for tensor type (use in GPUs). Different from findiff, the autodiff works on the chain rule of the differentials with two modes, forward accumulation and reverse accumulation [84, 85].

We choose the initial $\boldsymbol{\theta}$ randomly and iteratively optimize the cost function as shown in the results in the main figure 6. Among the three optimizes, the QNG converges fastest while the Adam results in a less stable near the optimal value, and the GD fluctuates in the first several iterations then towards the optimal value without fluctuating. This observation reveals the natural features of these optimizers [86–88]. The optimal values $\boldsymbol{\theta}^*$ and the optimal cost function are given in Tab. III. The results are plotted at $N = 100$, and the custom learning rate η for each optimizer are shown in the main figure 6. See the full code in G.

Table III. Optimal parameters $\boldsymbol{\theta}$ and its respective cost values for each optimizer.

Algorithm	θ_1	θ_2	θ_3	$\mathcal{C}(\boldsymbol{\theta})$
GD	-0.06292	0.07942	-0.02455	0.02273
ADAM	-0.03632	0.10609	0.00115	0.02622
QNG	-0.08166	0.11887	0.01525	0.03895

In addition, we compare the running time through the iteration for two types of devices: CPU and GPU. It can be seen from the inset figure 6 that the GPU runs faster than the CPU. The reason is that the autodiff in GPUs is more optimized than the findiff approximation in CPUs. The autodiff only calculates the cost function once and uses the reverse accumulation for calculating the gradient. Whereas the findiff needs to calculate the partial derivative for every θ_i , where for each θ_i , the cost function is computed twice: once for $\theta_i + \epsilon$ and once for $\theta_i - \epsilon$ (see Eq. (32).) Moreover, the findiff is difficult to convert, leading to inefficient code and intractable to perform higher order derivatives resulting in complexity and high error rate. The autodiff, however, can overcome these limitations.

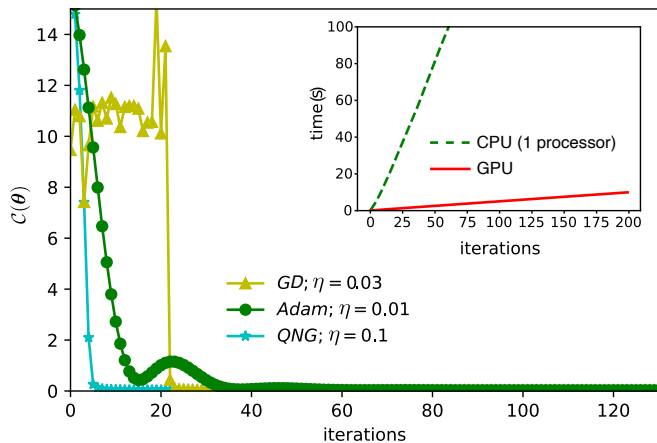


Figure 6. Plot of the cost function versus the number of iterations for different optimizers and learning rates. Among these optimizers, the QNG requires the smallest number of iterations to achieve convergence, the Adam is not stable near the optimal point, while the GD is unstable initially but quickly drops to the optimal value. Inset: comparing the execution times between the CPU and GPU devices.

B. Quantum phase transition

Quantum phase transition (QPT) is a transition between different quantum phases, such as the change in the ground state phases under the variation of magnetic fields (see [7] for reference.) Let us consider the Lipkin-Meshkov-Glick (LMG) model for an ensemble spins system interacting through a spin-spin infinite-range exchange coupling λ and exposing under an effective transverse field h . The interaction Hamiltonian is given by [89]

$$H_{\text{LMG}} = -2hJ_z - \frac{2\lambda}{N}(J_x^2 - J_y^2). \quad (33)$$

Due to the spin-spin interaction, the system may exhibit the quantum phase transition under the adiabatic dynamics [90–92].

We illustrate the QPT using `tcqix.pis` library. Let us set the ratio $r = h/\lambda$ for a fixed λ , and recast Eq. (33) as

$$H_{\text{LMG}} = -2\lambda \left[rJ_z + \frac{1}{N}(J_x^2 - J_y^2) \right]. \quad (34)$$

Its unitary evolution is given in terms of quantum gates as

$$U_{\text{LMG}} = e^{-itH_{\text{LMG}}} \approx e^{-i\lambda' r J_z} e^{-i\frac{\lambda'}{N}(J_x^2 - J_y^2)} = \text{RZ}(\Lambda r) \text{TAT}(\Lambda/N, 'xy'), \quad (35)$$

where we ignored higher order terms in t , i.e., the interaction time is short, and used $\Lambda = -2t\lambda$.

The results are shown in Fig. 7 for the first- and second-order of the expectation values, i.e., $\langle J_z \rangle$, $\langle J_x^2 \rangle$, and $\langle J_y^2 \rangle$. We fixed $\Lambda = -0.2$. We observe the phase transition as

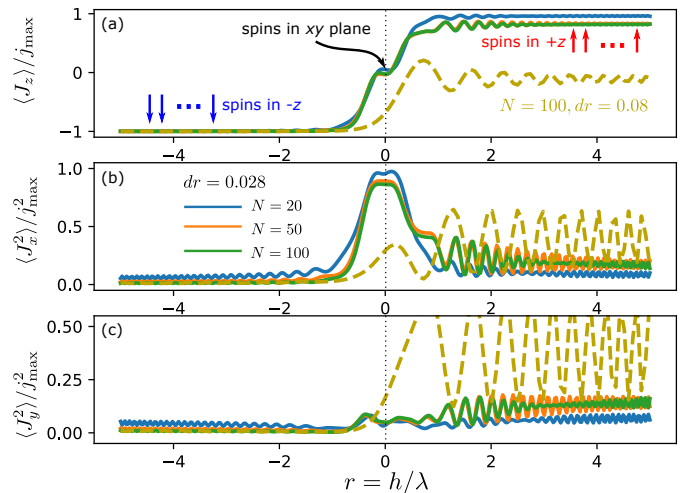


Figure 7. Quantum phase transition in the ensemble spins system via the change in expectation values when h changes its sign from minus to plus.

the change in these expectation values when the external transverse field h changes its sign (the solid curves,) which is similar to the previous study [21]. For example, in figure (a), starting from a negative $h < 0$, all the spins align along the $-z$ direction, i.e., the ground state dominated by the transverse field. Adiabatically changing h to the critical point, i.e., $h = 0$, then all the spins order in the xy plane. Continuing increasing h up to positive, all the spins align along the $+z$ direction, i.e., the phase completely changes.

To observe the QPT, we must choose the appropriate annealing time via r -step (dr), according to the adiabatic annealing evolution [93, 94]. The annealing time dr is defined by $dr = \frac{r_{\text{max}} - r_{\text{min}}}{T}$, T is the total time. We used $dr = 0.028$ (solid curves) in the above example and observed the QPT. If the annealing time is larger, e.g., $dr = 0.08$ (dashed curves), then the expectation values oscillate after the critical point. Detailed code is given in H.

VI. CONCLUSION

We developed `tcqix.pis`, an object-oriented library for quantum dynamics simulation of spin ensemble in Dicke basis. We applied the collective process in the ensemble of spin-1/2 particles and thus reduced the dimension of the whole system. The library allows for simulating quantum dynamics with collective states and collective operators. Furthermore, it integrates parallelizing multi-core processors and Graphics Processing Units, making it run faster. We finally showed two representative applications on quantum squeezing and quantum phase transition. Our library is a practical tool for simulating collective phenomena in ensemble systems with low computational cost, and we look forward near future

applications in many-body quantum dynamics.

DECLARATION OF COMPETING INTEREST

The authors declare that they have no known competing financial interests or personal relationships that could have appeared to influence the work reported in this paper.

ACKNOWLEDGMENT

This work is supported by the Ensemble Grants for Early Career Researches in Tohoku University.

AUTHOR CONTRIBUTIONS

Nguyen Tan Viet: wrote and implemented the code and performed the numerical calculations. **Nguyen Thi Chuong:** benchmarked and compared various libraries. **Vu Thi Ngoc Huyen:** proposed and analyzed the application on quantum phase transition. **Le Bin Ho:** proposed the theoretical framework, designed the model, and scrutinized the results. All authors discussed and contributed to the final manuscript.

Appendix A: An example code for employing a quantum circuit in `qutip.pis`

In `tqix.pis` to create a quantum circuit, we call `circuit` function, where `circuit.state` is a sparse matrix representation for the initial quantum state. The action of quantum gates on the state is given by `circuit.gate_name`, while the measurement is executed by `circuit.measure(num_shots)`.

```
from tqix import *
from tqix.pis import *
import numpy as np

numq=50

#call the initial circuit
qc = circuit(numq)
psi = qc.state
#print psi
print(psi) #sparse matrix
print(psi.toarray()) #full matrix

#apply the rotation gate RN on the circuit
qc.RN(-np.pi/2,np.pi/4)
psi2 = qc.state

#visualize state
THETA = [0, np.pi]
PHI = [0, 2* np.pi]
```

```
husimi_spin_3d(psi.toarray()+psi2.toarray(),
              THETA ,PHI, cmap = cmindex(1),dirname="./
              FIG",fname ="husimi_sphere.eps",view
              =(0,0))

#get probability
prob = qc.measure(num_shots=1000)
#plot figure
from matplotlib import pyplot as plt
x = np.arange(0,numq+1,1)
plt.bar(x,prob)
plt.savefig("./FIG/Pjm.eps")
```

Appendix B: Full code for producing Fig. 3 in the main text

```
from tqix.pis import *
from tqix import *
import time
import matplotlib.pyplot as plt

N_max=200 #max number of particles
L = 3 #number of layers

#run time benchmark on noiseless system
noiseless_time_qubits = []
for N in range(1,N_max):
    qc = circuit(N)

    start = time.time()

    for _ in range(L):
        qc.RX(np.pi/3)
        qc.RY(np.pi/3)
        qc.RZ(np.pi/3)

    noiseless_time = time.time()-start
    noiseless_time_qubits.append(
        noiseless_time)

#run time benchmark on noise system with #1
process for simulating noise
noise_time_qubits = []
for N in range(1,N_max):
    qc = circuit(N)

    start = time.time()

    for _ in range(L):
        qc.RX(np.pi/3,noise=0.05)
        qc.RY(np.pi/3,noise=0.05)
        qc.RZ(np.pi/3,noise=0.05)

    noise_time = time.time()-start
    noise_time_qubits.append(noise_time)

#run time benchmark on noise system with #
multi-processes for simulating noise
mp_noise_time_qubits = []
for N in range(1,N_max):
```

```

qc = circuit(N,num_process=25)

start = time.time()

for _ in range(L):
    qc.RX(np.pi/3,noise=0.05)
    qc.RY(np.pi/3,noise=0.05)
    qc.RZ(np.pi/3,noise=0.05)

mp_noise_time = time.time()-start
mp_noise_time_qubits.append(mp_noise_time)

#run time benchmark on noise system with #gpu
for simulating noise
gpu_noise_time_qubits = []
for N in range(1,N_max):
    qc = circuit(N,use_gpu=True)

    start = time.time()

    for _ in range(L):
        qc.RX(np.pi/3,noise=0.05)
        qc.RY(np.pi/3,noise=0.05)
        qc.RZ(np.pi/3,noise=0.05)

    gpu_noise_time = time.time()-start
    gpu_noise_time_qubits.append(
        gpu_noise_time)

#plot data
plt.plot(range(1,len(noiseless_time_qubits)
+1), noiseless_time_qubits, label = "
noiseless")
plt.plot(range(1,len(noise_time_qubits)+1),
noise_time_qubits, label = "noise (#
process = 1)")
plt.plot(range(1,len(mp_noise_time_qubits)+1)
, mp_noise_time_qubits, label = "noise (#
process = 25)")
plt.plot(range(1,len(gpu_noise_time_qubits)
+1), gpu_noise_time_qubits, label = "
noise (GPU: NVIDIA V100)")
plt.legend()
plt.show()
plt.savefig("figtimebm.eps")

```

Appendix C: Time complexity in a quantum gate execution

We categorize four cases of acting quantum gates on states and compute the time complexities \mathcal{O} (big O) as follows. We consider the “worse case” for every evaluation.

+ Case 1: **Noiseless and symmetry state.** The complexity for creating an operator J is $\mathcal{O}(N^2)$. The complexity for the state evolution with e^{-itJ} is $\mathcal{O}(N^3)$. The complexity for computing the density state in Eq. (24) is $\mathcal{O}(N^2)$. In total, the time complexity for this case is $\mathcal{O}(N^3)$.

+ Case 2: **Noiseless and collective state.** In the collective form, the cost of creating J is the total cost of creating block matrices (as in Fig. 1), each has $\mathcal{O}(i^2)$ with $i \in [j_{min}, \frac{N}{2}]$, so creating J costs $\mathcal{O}(N^3)$. The evolution of the state with e^{-itJ} costs $\mathcal{O}((d_N^j)^3) = \mathcal{O}(N^6)$. Therefore, the time complexity for this case is $\mathcal{O}(N^6)$.

+ Case 3: **Noise and symmetry state.** The first stage in this case is the same as case 1, so the time complexity is $\mathcal{O}(N^3)$. When adding noise, we have to process $\mathcal{O}(N^2)$ elements in the block- $\frac{N}{2}$. Each element costs $\mathcal{O}((d_N^j)^2) = \mathcal{O}(N^4)$. In total, the time complexity of the noise process is $\mathcal{O}(N^4 N^2) = \mathcal{O}(N^6)$.

+ Case 4: **Noise and collective state.** The procedure is the same as case 3 but we have to calculate all elements that are non-zeros in all block matrices, we have $\mathcal{O}(N^3)$ elements, each element costs $\mathcal{O}(N^4)$. Therefore, the time complexity is $\mathcal{O}(N^7)$.

Appendix D: Full code for producing Fig. 4 in the main text

```

from matplotlib import pyplot as plt
import numpy as np
import pickle

lb_res = pickle.load(open("./lib_benc_data.
pickle", "rb")) #load time data
benchmarked # for libraries
ax = plt.gca()
ax.plot(range(1, len(lb_res["tqix"])+1), np.log(
lb_res["tqix"]), 'b-*', label=r'$tqix$')
ax.plot(range(1, len(lb_res["qsun"])+1), np.log(
lb_res["qsun"]), 'g--^', label=r'$qsun$')
ax.plot(range(1, len(lb_res["qulacs"])+1), np.
log(lb_res["qulacs"]), 'r--o', label=r'$
qulacs$')
ax.plot(range(1, len(lb_res["yao"])+1), np.log(
lb_res["yao"]), 'c-.', label=r'$yao$')
ax.plot(range(1, len(lb_res["qiskit"])+1), np.
log(lb_res["qiskit"]), 'm-+', label=r'$
qiskit$')
ax.plot(range(1, len(lb_res["pennylane"])+1),
np.log(lb_res["pennylane"]), 'y--x', label=
r'$pennylane$')
ax.plot(range(1, len(lb_res["projectQ"])+1), np.
log(lb_res["projectQ"]), 'k-1', label=r'$
projectQ$')
ax.plot(range(1, len(lb_res["pyquil"])+1), np.
log(lb_res["pyquil"]), 'c--v', label=r'$
pyquil$')
ax.plot(range(1, len(lb_res["cirq"])+1), np.log(
lb_res["cirq"]), 'g->', label=r'$cirq$')
ax.plot(range(1, len(lb_res["qsim"])+1), np.log(
lb_res["qsim"]), 'y-3', label=r'$qsim$')
ax.plot(range(1, len(lb_res["quest"])+1), np.
log(lb_res["quest"]), 'm-s', label=r'$
quest$')

ax.set_xlabel("number of particles")
ax.set_ylabel("time execution (log scale)")

```

```
lgd = ax.legend(loc='center left',
               bbox_to_anchor=(1, 0.5))
plt.savefig("./lib_benchmark.eps",
           bbox_extra_artists=(lgd,), bbox_inches='
           tight')
```

Appendix E: Full code for producing Fig. 5 in the main text

```
from tqix.pis import *
from tqix import *
import numpy as np
from matplotlib import pyplot as plt
import os
N=100
THETA = [0, np.pi]
PHI = [0, 2* np.pi]
angles = np.linspace(0,0.5,100).tolist()

if os.path.isdir("./OAT"):
    pass
else:
    os.mkdir("./OAT")

if os.path.isdir("./TNT"):
    pass
else:
    os.mkdir("./TNT")

if os.path.isdir("./GMS"):
    pass
else:
    os.mkdir("./GMS")

if os.path.isdir("./TAT"):
    pass
else:
    os.mkdir("./TAT")

# OAT
OAT_xi_2_S = []
OAT_xi_2_R = []
for theta in angles:
    qc = circuit(N)
    qc.RN(np.pi/2,0)
    qc.OAT(theta,"Z")
    OAT_xi_2_S.append(10*np.log10(np.real(
    get_xi_2_S(qc))))
    OAT_xi_2_R.append(10*np.log10(np.real(
    get_xi_2_R(qc))))

# plot sphere
for theta in ([0.0, 0.02, 0.04, 0.06,
0.08,0.1]):
    qc = circuit(N)
    qc.RN(np.pi/2,0)
    qc.OAT(theta,"Z")
    husimi_spin_3d(qc.state.toarray(), THETA
    ,PHI ,cmap = cmindex(1),dirname="./OAT",
    fname =str(theta)+"husimi_sphere.eps",
    view=(180,0))
```

```
#TNT
TNT_xi_2_S = []
TNT_xi_2_R = []

for theta in angles:
    qc = circuit(N)
    qc.RN(np.pi/2,0)
    omega = N*theta
    qc.TNT(theta,omega=omega,gate_type="ZX"
    )
    TNT_xi_2_S.append(10*np.log10(np.real(
    get_xi_2_S(qc))))
    TNT_xi_2_R.append(10*np.log10(np.real(
    get_xi_2_R(qc))))

# plot sphere
for theta in ([0.0, 0.02, 0.04, 0.06,
0.08,0.1]):
    qc = circuit(N)
    qc.RN(np.pi/2,0)
    qc.TNT(theta,"ZX")
    husimi_spin_3d(qc.state.toarray(), THETA
    ,PHI ,cmap = cmindex(1),dirname="./TNT",
    fname =str(theta)+"husimi_sphere.eps",
    alpha=1,view=(180,0))

#GMS
GMS_xi_2_S = []
GMS_xi_2_R = []
phi = np.pi/4
for theta in angles:
    qc = circuit(N)
    qc.GMS(theta,phi)
    GMS_xi_2_S.append(10*np.log10(np.real(
    get_xi_2_S(qc))))
    GMS_xi_2_R.append(10*np.log10(np.real(
    get_xi_2_R(qc))))

# plot sphere
for theta in ([0.0, 0.02, 0.04, 0.06,
0.08,0.1]):
    qc = circuit(N)
    qc.GMS(theta,phi)
    husimi_spin_3d(qc.state.toarray(), THETA
    ,PHI ,cmap = cmindex(1),dirname="./GMS",
    fname =str(theta)+"husimi_sphere.eps",
    view=(-90,0))

# TAT
TAT_xi_2_S = []
TAT_xi_2_R = []
for theta in angles:
    qc = circuit(N)
    qc.RN(np.pi/2,0)
    qc.TAT(theta,"ZY")
    TAT_xi_2_S.append(10*np.log10(np.real(
    get_xi_2_S(qc))))
    TAT_xi_2_R.append(10*np.log10(np.real(
    get_xi_2_R(qc))))

# plot sphere
for theta in ([0.0, 0.02, 0.04, 0.06,
0.08,0.1]):
```

```

qc = circuit(N)
qc.RN(np.pi/2, 0)
qc.TAT(theta, "ZY")
husimi_spin_3d(qc.state.toarray(), THETA
, PHI , cmap = cmindex(1), dirname=". /TAT",
fname =str(theta)+"husimi_sphere.eps",
view=(180, 0))

ax = plt.gca()
ax.plot(angles, OAT_xi_2_S, 'c-o', label=r'
$10log_{10}(\xi^2_S)$-OAT$')
ax.plot(angles, TNT_xi_2_S, 'r-s', label=r'
$10log_{10}(\xi^2_S)$-TNT$')
ax.plot(angles, TAT_xi_2_S, 'g-*', label=r'
$10log_{10}(\xi^2_S)$-TAT$')
ax.plot(angles, GMS_xi_2_S, 'y-o', label=r'
$10log_{10}(\xi^2_S)$-GMS$')
ax.plot(angles, OAT_xi_2_R, 'c--o', label=r'
$10log_{10}(\xi^2_R)$-OAT$')
ax.plot(angles, TNT_xi_2_R, 'r--s', label=r'
$10log_{10}(\xi^2_R)$-TNT$')
ax.plot(angles, TAT_xi_2_R, 'g--*', label=r'
$10log_{10}(\xi^2_R)$-TAT$')
ax.plot(angles, GMS_xi_2_R, 'y--o', label=r'
$10log_{10}(\xi^2_R)$-GMS$')

ax.set_xlabel("theta")
ax.set_ylabel("Db")
lgd = ax.legend(loc='center left',
bbox_to_anchor=(1, 0.5))
dirname= ""
fname = "xi_2_S_R_graph.eps"
plt.savefig(os.path.join(dirname, fname))
plt.close()

```

Appendix F: Optimizers used in variation quantum squeezing circuit

In a variational circuit, the quantum part is parameterized by θ that will be iteratively updated by, such as gradient-based optimizers. Here, we consider the gradient descent (GD), Adam [95], and Quantum natural gradient (QNG) [86] optimizers. The GD computes new parameters via

$$\theta^{t+1} = \theta^t - \eta \nabla_{\theta} \mathcal{C}(\theta), \quad (\text{F1})$$

where $\nabla_{\theta} \mathcal{C}(\theta)$ is the gradient of $\mathcal{C}(\theta)$, and η is the learning rate. It is simple, but the coverage is low, and one must choose a proper learning rate to have the best result. Whereas, the Adam computes new parameters by

$$\theta^{t+1} = \theta^t - \eta \frac{\hat{m}_t}{\sqrt{\hat{v}_t + \epsilon}}, \quad (\text{F2})$$

where $m_t = \beta_1 m_{t-1} + (1 - \beta_1) \nabla_{\theta} \mathcal{C}(\theta)$, $v_t = \beta_2 v_{t-1} + (1 - \beta_2) \nabla_{\theta}^2 \mathcal{C}(\theta)$, $\hat{m}_t = m_t / (1 - \beta_1^t)$, $\hat{v}_t = v_t / (1 - \beta_2^t)$, with $\eta = 0.01$, $\beta_1 = 0.8$, $\beta_2 = 0.999$ and $\epsilon = 10^{-10}$. The Adam optimizer automatically adapts the learning rate and fast coverage, but it is noisy near the optimal point. Finally,

the QNG is better than other optimizers but requires more computational cost regards to quantum circuits. It is given by

$$\theta^{t+1} = \theta^t - \eta g^+ \nabla_{\theta} \mathcal{C}(\theta), \quad (\text{F3})$$

where g^+ is the pseudo-inverse of a Fubini-Study metric tensor g [86]. Detailed for deriving the Fubini-Study metric tensor can be seen from Ref. [88].

Appendix G: Full code for producing Fig. 6 in the main text

```

from tqix.pis import *
from tqix import *
import numpy as np
from matplotlib import pyplot as plt
import torch
import numpy as np

def cost_function(theta, use_gpu=False):
    qc = circuit(N, use_gpu=use_gpu)
    qc.RN(np.pi/2, 0)
    qc.OAT(theta[0], "Z")
    qc.TNT(theta[1], omega=theta[1], gate_type="ZX")
    qc.TAT(theta[2], "ZY")
    if use_gpu:
        loss = torch.real(get_xi_2_S(qc))
    else:
        loss = np.real(get_xi_2_S(qc))
    return loss

N=100 #number of particles
route = (("RN2",), ("OAT", "Z"), ("TNT", "ZX"), ("TAT", "ZY")) #define layers for QNG
loss_dict = {}

#function to optimize circuit of sparse array
def sparse(optimizer, loss_dict, mode):
    objective_function = lambda params:
    cost_function(params)
    init_params = [0.00195902, 0.14166777,
0.01656466] #random init parameters
    _, _, _, loss_hist, time_iters = fit(
    objective_function, optimizer, init_params,
    return_loss_hist=True, return_time_iters =
    True)
    loss_dict[mode] = loss_hist
    return loss_dict, time_iters

#function to optimize circuit of tensor
def tensor(optimizer, loss_dict, mode):
    objective_function = lambda params:
    cost_function(params, use_gpu=True)
    init_params = [0.00195902, 0.14166777,
0.01656466] #random init parameters
    init_params = torch.tensor(init_params).
    to('cuda').requires_grad_()
    _, _, _, loss_hist, time_iters = fit(
    objective_function, optimizer, init_params,

```

```

return_loss_hist=True,return_time_iters =
True)
loss_dict[mode] = loss_hist
return loss_dict,time_iters

#QNG
optimizer = GD(lr=0.03,eps=1e-10,maxiter=200,
use_qng=True,route=route,tol=1e-19,N=N)
loss_dict,_ = tensor(optimizer,loss_dict,"
tensor_qng")

#GD
optimizer = GD(lr=0.0001,eps=1e-10,maxiter
=200,tol=1e-19,N=N)
loss_dict,_ = tensor(optimizer,loss_dict,"
tensor_gd")

#ADAM
optimizer = ADAM(lr=0.01,eps=1e-10,amsgrad=
False,maxiter=200)
loss_dict,sparse_times = sparse(optimizer,
loss_dict,"sparse_adam")

optimizer = ADAM(lr=0.001,eps=1e-10,amsgrad=
False,maxiter=200)
loss_dict,tensor_times = tensor(optimizer,
loss_dict,"tensor_adam")

#plot loss values with respect to iterations
ax = plt.gca()
ax.plot(range(len(loss_dict["tensor_qng"])),
loss_dict["tensor_qng"],'c-*',label=r'
$QNG;\eta=0.1$')
ax.plot(range(len(loss_dict["tensor_gd"])),
loss_dict["tensor_gd"],'y-^',label=r'
$GD
;\eta=0.03$')
ax.plot(range(len(loss_dict["tensor_adam"])),
loss_dict["tensor_adam"],'g-o',label=r'
$Adam;\eta=0.01$')

ax.set_xlabel("iterations")
ax.set_ylabel(r"$C(\theta)$")
ax.set_xlim(0,130)
ax.set_ylim(0,15)
lgd = ax.legend(loc='center left',
bbox_to_anchor=(1, 0.25))
plt.savefig("./loss_bm.eps",
bbox_extra_artists=(lgd,), bbox_inches='
tight')

#for compare running time between using
tensor #and sparse array structure, we
plot ADAM #as an example

cumsum_vqa_time_res_sparse =
np.cumsum(loss_dict['sparse_adam'])
cumsum_vqa_time_res_tensor = np.cumsum(
loss_dict['tensor_adam'])
ax = plt.gca()
ax.plot(range(len(cumsum_vqa_time_res_sparse)
),cumsum_vqa_time_res_sparse,'g--',label=
r'$CPU$')

```

```

ax.plot(range(len(cumsum_vqa_time_res_tensor)
),cumsum_vqa_time_res_tensor,'r-',label=r
'$GPU$')

ax.set_xlabel("iterations")
ax.set_ylabel("time(s)")
ax.set_ylim(0,100)
lgd = ax.legend(loc='upper right')
plt.savefig("./timetensorsparse.eps",
bbox_extra_artists=(lgd,), bbox_inches='
tight')

```

Appendix H: Full code for producing Fig. 7 in the main text

```

from tqix import *
from tqix.pis import *
import numpy as np
from matplotlib import pyplot as plt

N = [20, 50, 100]
figure, axis = plt.subplots(3, 1)
for i in N:
    qc = circuit(i, use_gpu = False)

    aveJz = [] #average J_z
    aveJx2 = [] #average J_x@J_x
    aveJy2 = [] #average J_y@J_y

    r_min = -5
    r_max = 5
    r_iter = 357 #dr = (r_min-r_max)/r_iter ~
0.028
    x = np.linspace(r_min,r_max,r_iter)
    lambda_p = -0.2

    for j in x:
        qc.RZ(lambda_p*j)
        qc.TAT(lambda_p/i,'xy')

        tr0 = qc.expval('Jz')/i*2
        tr1 = qc.expval('Jx2')/i**2*4
        tr2 = qc.expval('Jy2')/i**2*4

        aveJz.append(np.real(tr0))
        aveJx2.append(np.real(tr1))
        aveJy2.append(np.real(tr2))

    axis[0].plot(x,aveJz)
    axis[1].plot(x,aveJx2)
    axis[2].plot(x,aveJy2)

# change annealing time
i = 100 #particles
qc1 = circuit(i, use_gpu = False)

aveJz = []
aveJx2 = []
aveJy2 = []

r_iter = 125 #dr = 0.08

```

```
x = np.linspace(r_min,r_max,r_iter)
lambda_p = -0.2

for j in x:
    qc1.RZ(lambda_p*j)
    qc1.TAT(lambda_p/i,'xy')

    tr0 = qc1.expval('Jz')/i*2
    tr1 = qc1.expval('Jx2')/i**2*4
    tr2 = qc1.expval('Jy2')/i**2*4

    aveJz.append(np.real(tr0))
    aveJx2.append(np.real(tr1))
    aveJy2.append(np.real(tr2))

axis[0].plot(x,aveJz, '--')
axis[1].plot(x,aveJx2, '--')
axis[2].plot(x,aveJy2, '--')

plt.savefig("figQPT.eps")
```

As mentioned in the main text, we can observe the QPT by choosing the approximate r_{step} , from which resolve to the adiabatic annealing evolution.

Appendix I: Guide for running multi-core and GPU-Acceleration on chip Apple M1

It requires MacOS 12.3+ and an ARM Python installation. We can check them by:

```
import platform
platform.platform()

>> macOS-12.4-arm64-arm-64bit (OK)
>> macOS-11.8-x86_64-i386-64bit (NOT)
```

Switch to the terminal and create a new ARM environment using Anaconda:

```
CONDA_SUBDIR=osx-arm64 conda create -n ml
python=3.9 -c conda-forge
```

Modify the CONDA_SUBDIR variable to permanently use osx-arm64 for future use:

```
conda env config vars set CONDA_SUBDIR=osx-arm64
```

From here, we can switch between the two environments (base) and (ml):

```
conda activate
conda activate ml
```

In the (ml) environment, let's install the required libraries (including tqix and pyTorch) and run the codes above normally. For more detail, see: <https://towardsdatascience.com/gpu-acceleration-comes-to-pytorch-on-m1-macs-195c399efcc1>

We can confirm if the MPS is working in Python by:

```
import torch
torch.has_mps

>> True
```

In Fig 8, we compare the running time on chip Apple M1 Max with $\#process = 10$ and GPU. The system configuration is the same as in figure 3.

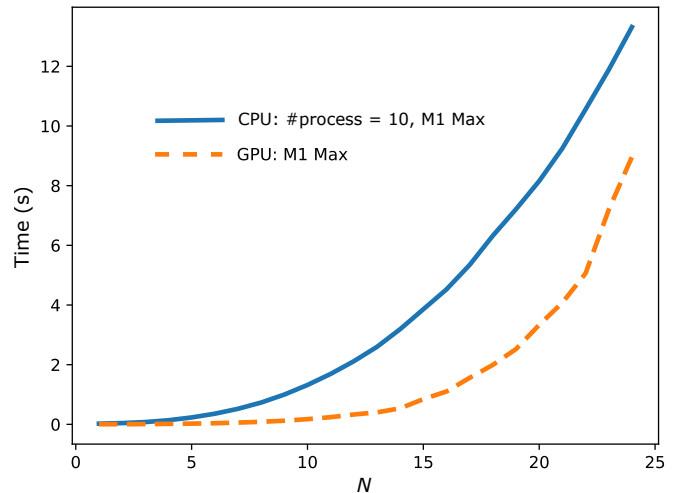


Figure 8. Benchmarking on chip Apple M1 Max with a comparison between the 10-processor CPU and the integrated GPU.

- [1] L. B. Ho, K. Q. Tuan, H. Q. Nguyen, tqix: A toolbox for quantum in x: X: Quantum measurement, quantum tomography, quantum metrology, and others, Computer Physics Communications 263 (2021) 107902. doi: <https://doi.org/10.1016/j.cpc.2021.107902>. URL <https://www.sciencedirect.com/science/article/pii/S001046552100045X>
- [2] R. H. Dicke, Coherence in spontaneous radiation processes, Phys. Rev. 93 (1954) 99–110. doi: [10.1103/PhysRev.93.99](https://doi.org/10.1103/PhysRev.93.99). URL <https://link.aps.org/doi/10.1103/PhysRev.93.99>
- [3] B. A. Chase, J. M. Geremia, Collective processes of an

ensemble of spin-1/2 particles, Phys. Rev. A 78 (2008) 052101. doi: [10.1103/PhysRevA.78.052101](https://doi.org/10.1103/PhysRevA.78.052101).

URL <https://link.aps.org/doi/10.1103/PhysRevA.78.052101>

- [4] J. Ma, X. Wang, C. Sun, F. Nori, Quantum spin squeezing, Physics Reports 509 (2) (2011) 89–165. doi: <https://doi.org/10.1016/j.physrep.2011.08.003>. URL <https://www.sciencedirect.com/science/article/pii/S0370157311002201>

- [5] R. Kaubruegger, P. Silvi, C. Kokail, R. van Bijnen, A. M. Rey, J. Ye, A. M. Kaufman, P. Zoller, Variational spin-squeezing algorithms on programmable quantum sensors, Phys. Rev. Lett. 123 (2019) 260505.

- doi:10.1103/PhysRevLett.123.260505.
 URL <https://link.aps.org/doi/10.1103/PhysRevLett.123.260505>
- [6] R. Kaubruegger, D. V. Vasilyev, M. Schulte, K. Hammerer, P. Zoller, Quantum variational optimization of ramsey interferometry and atomic clocks, *Phys. Rev. X* 11 (2021) 041045. doi:10.1103/PhysRevX.11.041045.
 URL <https://link.aps.org/doi/10.1103/PhysRevX.11.041045>
- [7] S. Sachdev, *Quantum Phase Transitions*, 2nd Edition, Cambridge University Press, 2011. doi:10.1017/CBO9780511973765.
- [8] A. Smith, M. S. Kim, F. Pollmann, J. Knolle, Simulating quantum many-body dynamics on a current digital quantum computer, *npj Quantum Information* 5 (1) (2019) 106. doi:10.1038/s41534-019-0217-0.
 URL <https://doi.org/10.1038/s41534-019-0217-0>
- [9] P. Schindler, D. Nigg, T. Monz, J. T. Barreiro, E. Martinez, S. X. Wang, S. Quint, M. F. Brandl, V. Nebendahl, C. F. Roos, M. Chwalla, M. Hennrich, R. Blatt, A quantum information processor with trapped ions, *New Journal of Physics* 15 (12) (2013) 123012. doi:10.1088/1367-2630/15/12/123012.
 URL <https://doi.org/10.1088/1367-2630/15/12/123012>
- [10] T. Hernández Yanes, M. Płodzień, M. Mackoít Sinkevičienė, G. Žilabys, G. Juzeliūnas, E. Witkowska, One- and two-axis squeezing via laser coupling in an atomic fermi-hubbard model, *Phys. Rev. Lett.* 129 (2022) 090403. doi:10.1103/PhysRevLett.129.090403.
 URL <https://link.aps.org/doi/10.1103/PhysRevLett.129.090403>
- [11] S. D. Bennett, N. Y. Yao, J. Otterbach, P. Zoller, P. Rabl, M. D. Lukin, Phonon-induced spin-spin interactions in diamond nanostructures: Application to spin squeezing, *Phys. Rev. Lett.* 110 (2013) 156402. doi:10.1103/PhysRevLett.110.156402.
 URL <https://link.aps.org/doi/10.1103/PhysRevLett.110.156402>
- [12] B. Q. Baragiola, B. A. Chase, J. Geremia, Collective uncertainty in partially polarized and partially decohered spin- $\frac{1}{2}$ systems, *Phys. Rev. A* 81 (2010) 032104. doi:10.1103/PhysRevA.81.032104.
 URL <https://link.aps.org/doi/10.1103/PhysRevA.81.032104>
- [13] V. V. Mikhailov, Multiplicities of angular momenta in a system of n-dimensional oscillators and the reduction $SU(n) \supset O(3)$, *Journal of Physics A: Mathematical and General* 11 (3) (1978) 443–456. doi:10.1088/0305-4470/11/3/006.
 URL <https://doi.org/10.1088/0305-4470/11/3/006>
- [14] L. Novo, T. Moroder, O. Gühne, Genuine multipartite entanglement of permutationally invariant states, *Phys. Rev. A* 88 (2013) 012305. doi:10.1103/PhysRevA.88.012305.
 URL <https://link.aps.org/doi/10.1103/PhysRevA.88.012305>
- [15] L. Arnaud, All possible permutational symmetries of a quantum system, *Phys. Rev. A* 93 (2016) 012320. doi:10.1103/PhysRevA.93.012320.
 URL <https://link.aps.org/doi/10.1103/PhysRevA.93.012320>
- [16] J. K. Stockton, J. M. Geremia, A. C. Doherty, H. Mabuchi, Characterizing the entanglement of symmetric many-particle spin- $\frac{1}{2}$ systems, *Phys. Rev. A* 67 (2003) 022112. doi:10.1103/PhysRevA.67.022112.
 URL <https://link.aps.org/doi/10.1103/PhysRevA.67.022112>
- [17] L.-M. Duan, M. D. Lukin, J. I. Cirac, P. Zoller, Long-distance quantum communication with atomic ensembles and linear optics, *Nature* 414 (6862) (2001) 413–418. doi:10.1038/35106500.
 URL <https://doi.org/10.1038/35106500>
- [18] L. M. Duan, J. I. Cirac, P. Zoller, Three-dimensional theory for interaction between atomic ensembles and free-space light, *Phys. Rev. A* 66 (2002) 023818. doi:10.1103/PhysRevA.66.023818.
 URL <https://link.aps.org/doi/10.1103/PhysRevA.66.023818>
- [19] M. Kitagawa, M. Ueda, Squeezed spin states, *Phys. Rev. A* 47 (1993) 5138–5143. doi:10.1103/PhysRevA.47.5138.
 URL <https://link.aps.org/doi/10.1103/PhysRevA.47.5138>
- [20] J. Hald, J. L. Sørensen, C. Schori, E. S. Polzik, Spin squeezed atoms: A macroscopic entangled ensemble created by light, *Phys. Rev. Lett.* 83 (1999) 1319–1322. doi:10.1103/PhysRevLett.83.1319.
 URL <https://link.aps.org/doi/10.1103/PhysRevLett.83.1319>
- [21] S. Morrison, A. S. Parkins, Dynamical quantum phase transitions in the dissipative lipkin-meshkov-glick model with proposed realization in optical cavity qed, *Phys. Rev. Lett.* 100 (2008) 040403. doi:10.1103/PhysRevLett.100.040403.
 URL <https://link.aps.org/doi/10.1103/PhysRevLett.100.040403>
- [22] C. Emary, T. Brandes, Quantum chaos triggered by precursors of a quantum phase transition: The dicke model, *Phys. Rev. Lett.* 90 (2003) 044101. doi:10.1103/PhysRevLett.90.044101.
 URL <https://link.aps.org/doi/10.1103/PhysRevLett.90.044101>
- [23] Y. K. Wang, F. T. Hioe, Phase transition in the dicke model of superradiance, *Phys. Rev. A* 7 (1973) 831–836. doi:10.1103/PhysRevA.7.831.
 URL <https://link.aps.org/doi/10.1103/PhysRevA.7.831>
- [24] H. Carmichael, C. Gardiner, D. Walls, Higher order corrections to the dicke superradiant phase transition, *Physics Letters A* 46 (1) (1973) 47–48. doi:https://doi.org/10.1016/0375-9601(73)90679-8.
 URL <https://www.sciencedirect.com/science/article/pii/0375960173906798>
- [25] C. Emary, T. Brandes, Chaos and the quantum phase transition in the dicke model, *Phys. Rev. E* 67 (2003) 066203. doi:10.1103/PhysRevE.67.066203.
 URL <https://link.aps.org/doi/10.1103/PhysRevE.67.066203>
- [26] J. M. Radcliffe, Some properties of coherent spin states, *Journal of Physics A: General Physics* 4 (3) (1971) 313–323. doi:10.1088/0305-4470/4/3/009.
 URL <https://doi.org/10.1088/0305-4470/4/3/009>
- [27] F. T. Arecchi, E. Courtens, R. Gilmore, H. Thomas,

- Atomic coherent states in quantum optics, *Phys. Rev. A* 6 (1972) 2211–2237. doi:10.1103/PhysRevA.6.2211.
URL <https://link.aps.org/doi/10.1103/PhysRevA.6.2211>
- [28] A. S. Sørensen, K. Mølmer, Entanglement and extreme spin squeezing, *Phys. Rev. Lett.* 86 (2001) 4431–4434. doi:10.1103/PhysRevLett.86.4431.
URL <https://link.aps.org/doi/10.1103/PhysRevLett.86.4431>
- [29] A. Sørensen, L.-M. Duan, J. I. Cirac, P. Zoller, Many-particle entanglement with bose-einstein condensates, *Nature* 409 (6816) (2001) 63–66. doi:10.1038/35051038.
URL <https://doi.org/10.1038/35051038>
- [30] A. Søndberg Sørensen, Bogoliubov theory of entanglement in a bose-einstein condensate, *Phys. Rev. A* 65 (2002) 043610. doi:10.1103/PhysRevA.65.043610.
URL <https://link.aps.org/doi/10.1103/PhysRevA.65.043610>
- [31] C. Gross, T. Zibold, E. Nicklas, J. Estève, M. K. Oberthaler, Nonlinear atom interferometer surpasses classical precision limit, *Nature* 464 (7292) (2010) 1165–1169. doi:10.1038/nature08919.
URL <https://doi.org/10.1038/nature08919>
- [32] M. F. Riedel, P. Böhi, Y. Li, T. W. Hänsch, A. Sinatra, P. Treutlein, Atom-chip-based generation of entanglement for quantum metrology, *Nature* 464 (7292) (2010) 1170–1173. doi:10.1038/nature08988.
URL <https://doi.org/10.1038/nature08988>
- [33] A. S. Sørensen, K. Mølmer, Entangling atoms in bad cavities, *Phys. Rev. A* 66 (2002) 022314. doi:10.1103/PhysRevA.66.022314.
URL <https://link.aps.org/doi/10.1103/PhysRevA.66.022314>
- [34] M. Schulte, V. J. Martínez-Lahuerta, M. S. Scharnagl, K. Hammerer, Ramsey interferometry with generalized one-axis twisting echoes, *Quantum* 4 (2020) 268. doi:10.22331/q-2020-05-15-268.
URL <https://doi.org/10.22331/q-2020-05-15-268>
- [35] J. Borregaard, E. J. Davis, G. S. Bentsen, M. H. Schleier-Smith, A. S. Sørensen, One- and two-axis squeezing of atomic ensembles in optical cavities, *New Journal of Physics* 19 (9) (2017) 093021. doi:10.1088/1367-2630/aa8438.
URL <https://doi.org/10.1088/1367-2630/aa8438>
- [36] M. Wang, W. Qu, P. Li, H. Bao, V. Vuletić, Y. Xiao, Two-axis-twisting spin squeezing by multipass quantum erasure, *Phys. Rev. A* 96 (2017) 013823. doi:10.1103/PhysRevA.96.013823.
URL <https://link.aps.org/doi/10.1103/PhysRevA.96.013823>
- [37] G. Liu, Y.-N. Wang, L.-F. Yan, N.-Q. Jiang, W. Xiong, M.-F. Wang, Spin squeezing via one- and two-axis twisting induced by a single off-resonance stimulated raman scattering in a cavity, *Phys. Rev. A* 99 (2019) 043840. doi:10.1103/PhysRevA.99.043840.
URL <https://link.aps.org/doi/10.1103/PhysRevA.99.043840>
- [38] Y. C. Liu, Z. F. Xu, G. R. Jin, L. You, Spin squeezing: Transforming one-axis twisting into two-axis twisting, *Phys. Rev. Lett.* 107 (2011) 013601. doi:10.1103/PhysRevLett.107.013601.
URL <https://link.aps.org/doi/10.1103/PhysRevLett.107.013601>
- [39] A. Micheli, D. Jaksch, J. I. Cirac, P. Zoller, Many-particle entanglement in two-component bose-einstein condensates, *Phys. Rev. A* 67 (2003) 013607. doi:10.1103/PhysRevA.67.013607.
URL <https://link.aps.org/doi/10.1103/PhysRevA.67.013607>
- [40] H. Strobel, W. Muessel, D. Linnemann, T. Zibold, D. B. Hume, L. Pezzè, A. Smerzi, M. K. Oberthaler, Fisher information and entanglement of non-gaussian spin states, *Science* 345 (6195) (2014) 424–427. arXiv:<https://www.science.org/doi/pdf/10.1126/science.1250147>, doi:10.1126/science.1250147.
URL <https://www.science.org/doi/abs/10.1126/science.1250147>
- [41] W. Muessel, H. Strobel, D. Linnemann, T. Zibold, B. Juliá-Díaz, M. K. Oberthaler, Twist-and-turn spin squeezing in bose-einstein condensates, *Phys. Rev. A* 92 (2015) 023603. doi:10.1103/PhysRevA.92.023603.
URL <https://link.aps.org/doi/10.1103/PhysRevA.92.023603>
- [42] C. K. Law, H. T. Ng, P. T. Leung, Coherent control of spin squeezing, *Phys. Rev. A* 63 (2001) 055601. doi:10.1103/PhysRevA.63.055601.
URL <https://link.aps.org/doi/10.1103/PhysRevA.63.055601>
- [43] K. Mølmer, A. Sørensen, Multiparticle entanglement of hot trapped ions, *Phys. Rev. Lett.* 82 (1999) 1835–1838. doi:10.1103/PhysRevLett.82.1835.
URL <https://link.aps.org/doi/10.1103/PhysRevLett.82.1835>
- [44] A. Sørensen, K. Mølmer, Quantum computation with ions in thermal motion, *Phys. Rev. Lett.* 82 (1999) 1971–1974. doi:10.1103/PhysRevLett.82.1971.
URL <https://link.aps.org/doi/10.1103/PhysRevLett.82.1971>
- [45] D. Maslov, Y. Nam, Use of global interactions in efficient quantum circuit constructions, *New Journal of Physics* 20 (3) (2018) 033018. doi:10.1088/1367-2630/aaa398.
URL <https://doi.org/10.1088/1367-2630/aaa398>
- [46] K. Groenland, F. Witteveen, K. Schoutens, R. Gerritsma, Signal processing techniques for efficient compilation of controlled rotations in trapped ions, *New Journal of Physics* 22 (6) (2020) 063006. doi:10.1088/1367-2630/ab8830.
URL <https://doi.org/10.1088/1367-2630/ab8830>
- [47] J. van de Wetering, Constructing quantum circuits with global gates, *New Journal of Physics* 23 (4) (2021) 043015. doi:10.1088/1367-2630/abf1b3.
URL <https://doi.org/10.1088/1367-2630/abf1b3>
- [48] M. Müller, K. Hammerer, Y. L. Zhou, C. F. Roos, P. Zoller, Simulating open quantum systems: from many-body interactions to stabilizer pumping, *New Journal of Physics* 13 (8) (2011) 085007. doi:10.1088/1367-2630/13/8/085007.
URL <https://doi.org/10.1088/1367-2630/13/8/085007>
- [49] O. Hosten, N. J. Engelsen, R. Krishnakumar, M. A.

- Kasevich, Measurement noise 100 times lower than the quantum-projection limit using entangled atoms, *Nature* 529 (7587) (2016) 505–508. doi:10.1038/nature16176.
URL <https://doi.org/10.1038/nature16176>
- [50] J. Huang, M. Zhuang, C. Lee, Non-gaussian precision metrology via driving through quantum phase transitions, *Phys. Rev. A* 97 (2018) 032116. doi:10.1103/PhysRevA.97.032116.
URL <https://link.aps.org/doi/10.1103/PhysRevA.97.032116>
- [51] S. A. Haine, J. J. Hope, Machine-designed sensor to make optimal use of entanglement-generating dynamics for quantum sensing, *Phys. Rev. Lett.* 124 (2020) 060402. doi:10.1103/PhysRevLett.124.060402.
URL <https://link.aps.org/doi/10.1103/PhysRevLett.124.060402>
- [52] T. J. Volkoff, M. J. Martin, Asymptotic optimality of twist-untwist protocols for heisenberg scaling in atom-based sensing, *Phys. Rev. Research* 4 (2022) 013236. doi:10.1103/PhysRevResearch.4.013236.
URL <https://link.aps.org/doi/10.1103/PhysRevResearch.4.013236>
- [53] Z. Li, B. Braverman, S. Colombo, C. Shu, A. Kawasaki, A. F. Adiyatullin, E. Pedrozo-Peñafiel, E. Mendez, V. Vuletić, Collective spin-light and light-mediated spin-spin interactions in an optical cavity, *PRX Quantum* 3 (2022) 020308. doi:10.1103/PRXQuantum.3.020308.
URL <https://link.aps.org/doi/10.1103/PRXQuantum.3.020308>
- [54] A. Kuzmich, K. Mølmer, E. S. Polzik, Spin squeezing in an ensemble of atoms illuminated with squeezed light, *Phys. Rev. Lett.* 79 (1997) 4782–4785. doi:10.1103/PhysRevLett.79.4782.
URL <https://link.aps.org/doi/10.1103/PhysRevLett.79.4782>
- [55] M. G. Moore, O. Zobay, P. Meystre, Quantum optics of a bose-einstein condensate coupled to a quantized light field, *Phys. Rev. A* 60 (1999) 1491–1506. doi:10.1103/PhysRevA.60.1491.
URL <https://link.aps.org/doi/10.1103/PhysRevA.60.1491>
- [56] M. Fleischhauer, S. Gong, Stationary source of nonclassical or entangled atoms, *Phys. Rev. Lett.* 88 (2002) 070404. doi:10.1103/PhysRevLett.88.070404.
URL <https://link.aps.org/doi/10.1103/PhysRevLett.88.070404>
- [57] S. A. Haine, M. K. Olsen, J. J. Hope, Generating controllable atom-light entanglement with a raman atom laser system, *Phys. Rev. Lett.* 96 (2006) 133601. doi:10.1103/PhysRevLett.96.133601.
URL <https://link.aps.org/doi/10.1103/PhysRevLett.96.133601>
- [58] S. S. Szigeti, B. Tonekaboni, W. Y. S. Lau, S. N. Hood, S. A. Haine, Squeezed-light-enhanced atom interferometry below the standard quantum limit, *Phys. Rev. A* 90 (2014) 063630. doi:10.1103/PhysRevA.90.063630.
URL <https://link.aps.org/doi/10.1103/PhysRevA.90.063630>
- [59] S. A. Haine, S. S. Szigeti, M. D. Lang, C. M. Caves, Heisenberg-limited metrology with information recycling, *Phys. Rev. A* 91 (2015) 041802. doi:10.1103/PhysRevA.91.041802.
URL <https://link.aps.org/doi/10.1103/PhysRevA.91.041802>
- [60] V. B. Braginsky, Y. I. Vorontsov, K. S. Thorne, Quantum nondemolition measurements, *Science* 209 (4456) (1980) 547–557. arXiv:<https://www.science.org/doi/pdf/10.1126/science.209.4456.547>, doi:10.1126/science.209.4456.547.
URL <https://www.science.org/doi/abs/10.1126/science.209.4456.547>
- [61] A. Kuzmich, L. Mandel, N. P. Bigelow, Generation of spin squeezing via continuous quantum nondemolition measurement, *Phys. Rev. Lett.* 85 (2000) 1594–1597. doi:10.1103/PhysRevLett.85.1594.
URL <https://link.aps.org/doi/10.1103/PhysRevLett.85.1594>
- [62] A. Louchet-Chauvet, J. Appel, J. J. Renema, D. Oblak, N. Kjaergaard, E. S. Polzik, Entanglement-assisted atomic clock beyond the projection noise limit, *New Journal of Physics* 12 (6) (2010) 065032. doi:10.1088/1367-2630/12/6/065032.
URL <https://doi.org/10.1088/1367-2630/12/6/065032>
- [63] D. Yang, A. Grankin, L. M. Sieberer, D. V. Vasilyev, P. Zoller, Quantum non-demolition measurement of a many-body hamiltonian, *Nature Communications* 11 (1) (2020) 775. doi:10.1038/s41467-020-14489-5.
URL <https://doi.org/10.1038/s41467-020-14489-5>
- [64] V. B. Braginsky, F. Y. Khalili, Quantum nondemolition measurements: the route from toys to tools, *Rev. Mod. Phys.* 68 (1996) 1–11. doi:10.1103/RevModPhys.68.1.
URL <https://link.aps.org/doi/10.1103/RevModPhys.68.1>
- [65] P. Grangier, J. A. Levenson, J.-P. Poizat, Quantum nondemolition measurements in optics, *Nature* 396 (6711) (1998) 537–542. doi:10.1038/25059.
URL <https://doi.org/10.1038/25059>
- [66] Z. Zhang, L.-M. Duan, Generation of massive entanglement through an adiabatic quantum phase transition in a spinor condensate, *Phys. Rev. Lett.* 111 (2013) 180401. doi:10.1103/PhysRevLett.111.180401.
URL <https://link.aps.org/doi/10.1103/PhysRevLett.111.180401>
- [67] X.-Y. Luo, Y.-Q. Zou, L.-N. Wu, Q. Liu, M.-F. Han, M. K. Tey, L. You, Deterministic entanglement generation from driving through quantum phase transitions, *Science* 355 (6325) (2017) 620–623. arXiv:<https://www.science.org/doi/pdf/10.1126/science.aag1106>, doi:10.1126/science.aag1106.
URL <https://www.science.org/doi/abs/10.1126/science.aag1106>
- [68] P. Feldmann, M. Gessner, M. Gabbriellini, C. Klempt, L. Santos, L. Pezzè, A. Smerzi, Interferometric sensitivity and entanglement by scanning through quantum phase transitions in spinor bose-einstein condensates, *Phys. Rev. A* 97 (2018) 032339. doi:10.1103/PhysRevA.97.032339.
URL <https://link.aps.org/doi/10.1103/PhysRevA.97.032339>
- [69] M. A. Nielsen, I. L. Chuang, *Quantum computation and quantum information*, Cambridge University Press, 2010.
- [70] N. Khammassi, I. Ashraf, X. Fu, C. Almudever, K. Ber-

- tels, Qx: A high-performance quantum computer simulation platform, in: Design, Automation & Test in Europe Conference & Exhibition (DATE), 2017, 2017, pp. 464–469. doi:10.23919/DATE.2017.7927034.
- [71] N. Shammah, S. Ahmed, N. Lambert, S. De Liberato, F. Nori, Open quantum systems with local and collective incoherent processes: Efficient numerical simulations using permutational invariance, *Phys. Rev. A* 98 (2018) 063815. doi:10.1103/PhysRevA.98.063815.
URL <https://link.aps.org/doi/10.1103/PhysRevA.98.063815>
- [72] L. B. Ho, H. Hakoshima, Y. Matsuzaki, M. Matsuzaki, Y. Kondo, Multiparameter quantum estimation under dephasing noise, *Phys. Rev. A* 102 (2020) 022602. doi:10.1103/PhysRevA.102.022602.
URL <https://link.aps.org/doi/10.1103/PhysRevA.102.022602>
- [73] Qsim: Quantum computer simulator toolkit, <https://quantumai.google/qsim>.
- [74] Cirq: A python framework for creating, editing, and invoking noisy intermediate scale quantum (nisq) circuits, <https://quantumai.google/cirq>.
- [75] Y. Suzuki, Y. Kawase, Y. Masumura, Y. Hiraga, M. Nakadai, J. Chen, K. M. Nakanishi, K. Mitarai, R. Imai, S. Tamiya, T. Yamamoto, T. Yan, T. Kawakubo, Y. O. Nakagawa, Y. Ibe, Y. Zhang, H. Yamashita, H. Yoshimura, A. Hayashi, K. Fujii, Qulacs: a fast and versatile quantum circuit simulator for research purpose, *Quantum* 5 (2021) 559. doi:10.22331/q-2021-10-06-559.
URL <https://doi.org/10.22331/q-2021-10-06-559>
- [76] X.-Z. Luo, J.-G. Liu, P. Zhang, L. Wang, Yao.jl: Extensible, Efficient Framework for Quantum Algorithm Design, *Quantum* 4 (2020) 341. doi:10.22331/q-2020-10-11-341.
URL <https://doi.org/10.22331/q-2020-10-11-341>
- [77] Q. C. Nguyen, L. B. Ho, L. N. Tran, H. Q. Nguyen, Qsun: an open-source platform towards practical quantum machine learning applications, *Machine Learning: Science and Technology* 3 (1) (2022) 015034. doi:10.1088/2632-2153/ac5997.
URL <https://doi.org/10.1088/2632-2153/ac5997>
- [78] T. Jones, A. Brown, I. Bush, S. C. Benjamin, Quest and high performance simulation of quantum computers, *Scientific Reports* 9 (1) (2019) 10736. doi:10.1038/s41598-019-47174-9.
URL <https://doi.org/10.1038/s41598-019-47174-9>
- [79] V. Bergholm, J. Izaac, M. Schuld, C. Gogolin, M. S. Alam, S. Ahmed, J. M. Arrazola, C. Blank, A. Delgado, S. Jahangiri, K. McKiernan, J. J. Meyer, Z. Niu, A. Száva, N. Killoran, PennyLane: Automatic differentiation of hybrid quantum-classical computations (2018). doi:10.48550/ARXIV.1811.04968.
URL <https://arxiv.org/abs/1811.04968>
- [80] Qiskit is an open-source framework for working with noisy quantum computers at the level of pulses, circuits, and algorithms., <https://qiskit.org>.
- [81] D. S. Steiger, T. Häner, M. Troyer, ProjectQ: an open source software framework for quantum computing, *Quantum* 2 (2018) 49. doi:10.22331/q-2018-01-31-49.
URL <https://doi.org/10.22331/q-2018-01-31-49>
- [82] Pyquil: Quantum programming in python., <https://pyquil-docs.rigetti.com/en/stable/index.html>.
- [83] D. J. Wineland, J. J. Bollinger, W. M. Itano, D. J. Heinzen, Squeezed atomic states and projection noise in spectroscopy, *Phys. Rev. A* 50 (1994) 67–88. doi:10.1103/PhysRevA.50.67.
URL <https://link.aps.org/doi/10.1103/PhysRevA.50.67>
- [84] M. Bartholomew-Biggs, S. Brown, B. Christianson, L. Dixon, Automatic differentiation of algorithms, *Journal of Computational and Applied Mathematics* 124 (1) (2000) 171–190, numerical Analysis 2000. Vol. IV: Optimization and Nonlinear Equations. doi:https://doi.org/10.1016/S0377-0427(00)00422-2.
URL <https://www.sciencedirect.com/science/article/pii/S0377042700004222>
- [85] R. D. Neidinger, Introduction to automatic differentiation and matlab object-oriented programming, *SIAM Review* 52 (3) (2010) 545–563. arXiv: <https://doi.org/10.1137/080743627>, doi:10.1137/080743627.
URL <https://doi.org/10.1137/080743627>
- [86] J. Stokes, J. Izaac, N. Killoran, G. Carleo, Quantum Natural Gradient, *Quantum* 4 (2020) 269. doi:10.22331/q-2020-05-25-269.
URL <https://doi.org/10.22331/q-2020-05-25-269>
- [87] T. Haug, M. S. Kim, Natural parameterized quantum circuit (2021). doi:10.48550/ARXIV.2107.14063.
URL <https://arxiv.org/abs/2107.14063>
- [88] V. T. Hai, L. B. Ho, Universal compilation for quantum state preparation and tomography (2022). doi:10.48550/ARXIV.2204.11635.
URL <https://arxiv.org/abs/2204.11635>
- [89] H. Lipkin, N. Meshkov, A. Glick, Validity of many-body approximation methods for a solvable model: (i). exact solutions and perturbation theory, *Nuclear Physics* 62 (2) (1965) 188–198. doi:https://doi.org/10.1016/0029-5582(65)90862-X.
URL <https://www.sciencedirect.com/science/article/pii/002955826590862X>
- [90] S. Dusuel, J. Vidal, Continuous unitary transformations and finite-size scaling exponents in the lipkin-meshkov-glick model, *Phys. Rev. B* 71 (2005) 224420. doi:10.1103/PhysRevB.71.224420.
URL <https://link.aps.org/doi/10.1103/PhysRevB.71.224420>
- [91] T. Caneva, R. Fazio, G. E. Santoro, Adiabatic quantum dynamics of the lipkin-meshkov-glick model, *Phys. Rev. B* 78 (2008) 104426. doi:10.1103/PhysRevB.78.104426.
URL <https://link.aps.org/doi/10.1103/PhysRevB.78.104426>
- [92] O. L. Acevedo, L. Quiroga, F. J. Rodríguez, N. F. Johnson, New dynamical scaling universality for quantum networks across adiabatic quantum phase transitions, *Phys. Rev. Lett.* 112 (2014) 030403. doi:10.1103/PhysRevLett.112.030403.
URL <https://link.aps.org/doi/10.1103/PhysRevLett.112.030403>

- [93] E. Farhi, J. Goldstone, S. Gutmann, J. Lapan, A. Lundgren, D. Preda, A quantum adiabatic evolution algorithm applied to random instances of an np-complete problem, *Science* 292 (5516) (2001) 472–475. arXiv:<https://www.science.org/doi/pdf/10.1126/science.1057726>, doi:10.1126/science.1057726. URL <https://www.science.org/doi/abs/10.1126/science.1057726>
- [94] D. Aharonov, W. van Dam, J. Kempe, Z. Landau, S. Lloyd, O. Regev, Adiabatic quantum computation is equivalent to standard quantum computation, *SIAM Review* 50 (4) (2008) 755–787. arXiv:<https://doi.org/10.1137/080734479>, doi:10.1137/080734479. URL <https://doi.org/10.1137/080734479>
- [95] D. P. Kingma, J. Ba, Adam: A method for stochastic optimization (2014). doi:10.48550/ARXIV.1412.6980. URL <https://arxiv.org/abs/1412.6980>